Satellite Navigation
https://satellite-navigation.springeropen.com/

ORIGINAL ARTICLE

Open Access

Monitoring and correction of errors in state space representation products using PPP float ambiguity deviations and phase residuals in a wide-area network

Yunqing Tian[1,2], Bao Shu[1*], Yuhang Zheng[1], Guillermo González-Casado[2], Yang Gao[3], Li Wang[1], Adria Rovira-Garcia[2], Guanwen Huang[1] and Qin Zhang[1]

Abstract

Real-time Precise Point Positioning with Ambiguity Resolution (PPP-AR) critically depends on high-quality State Space Representation (SSR) products for satellite orbit, clock, and code/phase bias corrections. These products, however, often contain errors that can severely degrade user positioning performance. Existing network-based quality monitoring methods primarily rely on phase residuals to detect product errors. However, phase residuals are only effective in revealing SSR product errors after ambiguities have been fixed. Before ambiguities are fixed, the stable or slowly varying components of SSR product errors are absorbed into the float ambiguities, rendering such phase residuals insufficient to fully reveal SSR product errors. As a result, the products with unfixed ambiguities are typically tagged as unreliable due to their uncertain quality. This practice however reduces the availability of SSR products and limit user PPP-AR performance, particularly in challenging environments where fewer satellites are visible. To address this limitation, this study proposes a method that effectively monitors SSR product quality by jointly considering the deviations of float ambiguities from their true integer values and phase residuals associated with float ambiguities. Unlike the ambiguity-fixed phase residuals, these indicators are derived directly from the float PPP solution and provide a unified measure of SSR product errors, regardless of whether the ambiguities remain float or are subsequently fixed. Furthermore, by leveraging the spatial common-mode characteristics of the SSR product errors across a wide-area network, the method derives the corrections to mitigate product error. After correction, the ambiguity-float phase residuals serve as a unified quality indicator applicable to both ambiguity-fixed and ambiguity-float SSR products, enabling reliable quality assessment and anomaly detection. Validation using one month of real-time SSR products from CNES demonstrates that the proposed method significantly improves the availability and reliability of SSR products. Compared with traditional monitoring methods based on ambiguity-fixed phase residuals, the proposed method achieves a comparable and slightly higher ambiguity fixing rate (95.56% versus 92.83%), while significantly reducing the incorrect fixing rate from 0.69 to 0.09%. This improvement substantially mitigates the positioning degradation caused by incorrect ambiguity fixing, reducing the three-dimensional Root Mean Square Error (RMSE) from 15.1 to 4.6 cm.

Keywords Real-time PPP, Ambiguity fixing, SSR product errors, Ambiguity deviations, Phase residuals, Quality monitoring

*Correspondence:
Bao Shu
baos613@chd.edu.cn
Full list of author information is available at the end of the article

Introduction

The State Space Representation (SSR) products consist of high-precision satellite orbit, clock, and code/phase bias corrections, which are essential for real-time Precise Point Positioning (PPP) with Ambiguity Resolution (PPP-AR) (Teunissen et al., 2010; Weber et al., 2007). Since PPP-AR operates in an undifferenced mode, any errors in SSR products will propagate directly into the user positioning model and subsequently degrade positioning performance (Liu et al., 2020; Xiao et al., 2025; Zhou et al., 2023). In practice, real-time SSR products inevitably contain errors that must be considered. For example, the Signal in Space Range Errors (SISREs) of real-time orbit and clock products of GPS and Galileo are typically 2–5 cm under nominal conditions but can exceed 14 cm during orbit maneuvers (Duan et al., 2019; Li et al., 2022). Phase bias corrections can also exhibit anomalies, with probabilities of about 0.1–2.0% (Duan et al., 2024). Monitoring the quality of the SSR products is therefore essential to ensure high precision and reliability of PPP-AR (Du et al., 2021; Wang & Shen, 2020).

To address this need, several methods have been developed to monitor the quality of the SSR products, aiming to evaluate product errors, detect anomalies, and enable proper weighting and flagging affected satellites. Among them, monitoring approaches based on station networks are widely used. The key to network-based approaches is to derive quality indicators in network processing that reliably reflect the SSR product errors. Early efforts focused primarily on monitoring orbit and clock errors. Some researchers have treated SSR product errors as additional estimable parameters in network PPP models, deriving product error estimates through multi-station joint processing (Huang et al., 2024; Ji et al., 2022). Another widely adopted approach computes phase residuals (observed-minus-computed phase values) from independent PPP processing at multiple stations, where these phase residuals serve as quality indicators of orbit and clock product errors (Wang & Shen, 2020; Weinbach et al., 2018; Xue et al., 2024; Zhou et al., 2025). These approaches performed well in detecting abrupt orbit and clock anomalies, significantly improving the reliability and accuracy of PPP positioning.

With the advancement of PPP-AR, researchers have recognized that monitoring the quality of phase biases is equally critical. Integer ambiguity resolution depends not only on high-quality orbit and clock products but also on precise phase bias products. Even slowly varying or stable errors can prevent ambiguities from being resolved to their correct integer values. Therefore, SSR quality monitoring must consider not only significant product anomalies or instabilities, but also whether the products preserve the integer nature required for ambiguity resolution. However, in float PPP solutions, float ambiguity parameters absorb part of the SSR errors (especially temporally stable or slowly varying), leaving only the unabsorbed portion visible in phase residuals. This prevents ambiguity-float phase residuals from fully revealing SSR product errors. Only after the ambiguities are fixed to integer values can the SSR product errors be fully revealed in phase residuals, rather than being partially absorbed by ambiguities. Therefore, ambiguity-fixed phase residuals have been widely adopted in monitoring SSR product quality (Li et al., 2024; Xie et al., 2025) and this strategy has been implemented in services such as QZSS CLAS (Fujita et al., 2016). Although ambiguity-fixed phase residual analysis effectively evaluates SSR product quality, its applicability is limited to ambiguity-fixed SSR products. For ambiguity-float SSR products, ambiguity-fixed phase residuals are unavailable, and these products are typically deemed unreliable and excluded from evaluation and subsequent use. In practice, failure in ambiguity fixing indicates reduced product reliability, but does not imply that the corresponding SSR products are entirely unusable. Discarding these ambiguity-float products may degrade user PPP-AR performance, especially in challenging environments with limited satellite visibility (e.g. urban canyons or ionospheric scintillation). Although ambiguity-float SSR products may still contain valuable information, the key challenge is how to properly characterize their quality for reliable screening and utilization.

To overcome this limitation, we propose a unified monitoring and correction method applicable to both ambiguity-fixed and ambiguity-float SSR products. Our approach is based on the recognition that in float PPP solutions, SSR product errors are partially absorbed by float ambiguity parameters, manifesting as deviations of float ambiguity estimates from their true integer values. The time-varying components that are not absorbed remain primarily in the ambiguity-float phase residuals. By jointly considering both float ambiguity deviations and ambiguity-float phase residuals, the absorbed SSR product error components can be recovered, enabling complete quantification of SSR product quality regardless of whether the ambiguities remain float or subsequently fixed. Furthermore, by leveraging the spatial common-mode characteristics of SSR errors across a wide-area network (Lou et al., 2014; Zheng et al., 2021) and the temporal stability of ambiguities, we perform multi-station joint modeling of float ambiguity deviations to estimate corrections for SSR product error mitigation. After correction, the ambiguity-float phase residuals can serve as unified quality indicators, applicable to both ambiguity-fixed and ambiguity-float SSR products, thereby enabling reliable anomaly detection and quality assessment.

The effectiveness of the proposed method is validated through multi-station experiments using real-time SSR products.

Methodology

The proposed method establishes a unified framework for monitoring and correcting errors in SSR products. As illustrated in Fig. 1, the method consists of two major components. In the first component, PPP float solutions are performed at multiple monitoring stations using the target SSR products. For each satellite, the float ambiguity deviations and the ambiguity-float phase residuals are extracted at each monitoring station. These two quantities jointly reflect the overall SSR product errors.

In the second component, the extracted float ambiguity deviations and the ambiguity-float phase residuals at all monitoring stations are analyzed through a two-step process. First, inter-station consistency checks for each satellite are performed separately on both quantities to eliminate outliers caused by local environmental effects or measurement noise. Second, the validated ambiguity deviations at multiple stations are jointly modeled to derive correction terms, which mitigate systematic and regionally common errors presented in the original SSR products. The ambiguity-float phase residuals are then used to assess the quality of the corrected SSR products. Since the error components absorbed by the ambiguity parameters have been largely mitigated through the derived corrections, the phase residuals predominantly represent the remaining uncorrected errors and therefore serve as the primary indicators for quality evaluation and anomaly detection. Ultimately, these outputs help improve PPP-AR user performance.

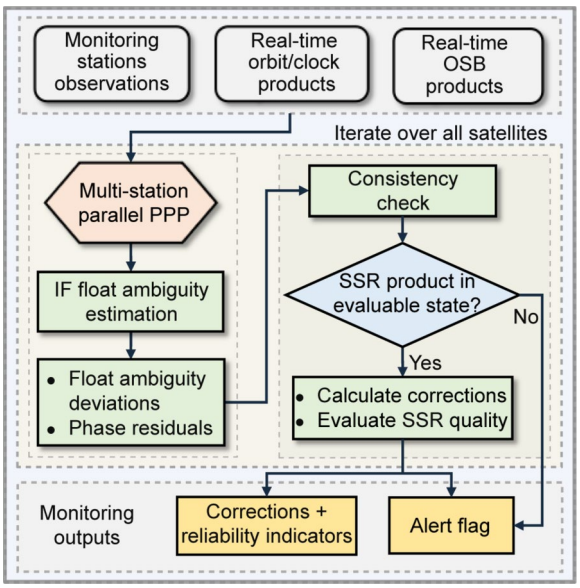

Fig. 1 Flowchart of the monitoring and correction method for SSR product errors

Extraction of combined SSR product errors

The Ionosphere-Free (IF) combination of dual-frequency GNSS signals eliminates first-order ionospheric delays. The IF code and phase observations can be written as (Li et al., 2021; Sanz et al., 2013):

$$\begin{cases} P^s_{r,\mathrm{IF}} = \rho^s_r + c(t_{r,\mathrm{IF}} - t^s_{\mathrm{IF}}) + m^s_h w_r + e^s_{\mathrm{IF}} \\ L^s_{r,\mathrm{IF}} = \rho^s_r + c(t_{r,IF} - t^s_{\mathrm{IF}}) + m^s_h w_r + \lambda_{\mathrm{IF}} \tilde{N}^s_{r,\mathrm{IF}} + \varepsilon^s_{\mathrm{IF}} \end{cases} \tag{1}$$

with

$$\begin{cases} t_{r,\mathrm{IF}} = t_r + b_{r,\mathrm{IF}}/c \\ t^s_{\mathrm{IF}} = t^s + b^s_{\mathrm{IF}}/c \\ \tilde{N}^s_{r,\mathrm{IF}} = N^s_{r,\mathrm{IF}} + (B_{r,\mathrm{IF}} - B^s_{\mathrm{IF}}) - (b_{r,\mathrm{IF}} - b^s_{\mathrm{IF}})/\lambda_{\mathrm{IF}} \end{cases} \tag{2}$$

where ρ is the geometric distance between satellite (s) and receiver (r); c is the speed of light in vacuum; $t_{r,\mathrm{IF}}$ and t^s_{IF} are the receiver and satellite clock offsets, respectively; w_r denotes the zenith troposphere wet delay with its mapping function m^s_h; $N^s_{r,\mathrm{IF}}$ refers to the IF combination ambiguity, and λ_{IF} is the IF combination equivalent wavelength; $b_{r,\mathrm{IF}}$ and b^s_{IF} denote IF code biases while $B_{r,\mathrm{IF}}$ and B^s_{IF} means IF phase biases of receiver and satellite, respectively; e^s_{IF} and $\varepsilon^s_{\mathrm{IF}}$ are code and phase observation noise, respectively.

At monitoring stations, the station coordinates are fixed, and the satellite orbits, clocks, and code/phase bias parameters are also fixed using precise products, such as those from IGS. In particular, the code and phase bias corrections in the IF model are derived from Observable-specific Signal Bias (OSB) products (Laurichesse, 2012):

$$\begin{cases} b^s_{\mathrm{igs,IF}} = \alpha_{i,j} b^s_{\mathrm{igs},i} + \beta_{i,j} b^s_{\mathrm{igs},j} = 0 \\ \lambda_{\mathrm{IF}} B^s_{\mathrm{igs,IF}} = \alpha_{i,j}\lambda_i B^s_{\mathrm{igs},i} + \beta_{i,j}\lambda_j B^s_{\mathrm{igs},j} = \lambda_{\mathrm{IF}} B^s_{\mathrm{IF}} - b^s_{\mathrm{IF}} \end{cases} \tag{3}$$

with

$$\alpha_{i,j} = \frac{f_i^2}{f_i^2 - f_j^2},\ \beta_{i,j} = \frac{-f_j^2}{f_i^2 - f_j^2} \tag{4}$$

where $\alpha_{i,j}$ and $\beta_{i,j}$ are the IF coefficients for frequencies f_i and f_j; $b^s_{\mathrm{igs},i}$ and $b^s_{\mathrm{igs},j}$ represent the code OSB products; $B^s_{\mathrm{igs},i}$ and $B^s_{\mathrm{igs},j}$ denote the phase OSB products. In general, the accuracy of real-time SSR products is much poorer than that of final or rapid products, even those from IGS (Li et al., 2022). The SSR product errors can be represented as:

$$\begin{cases} \boldsymbol{X}^s = \boldsymbol{X}^s_{\text{igs}} + \delta\boldsymbol{X}^s_{\text{igs}} \\ t^s_{\text{IF}} = t^s_{\text{igs,IF}} + \delta t^s_{\text{igs,IF}} \\ B^s_{\text{IF}} = B^s_{\text{igs,IF}} + \delta B^s_{\text{igs,IF}} \end{cases} \tag{5}$$

where $\boldsymbol{X}^s_{\text{igs}}$, $t^s_{\text{igs,IF}}$ and $B^s_{\text{igs,IF}}$ represent the IGS satellite orbit, clock, and phase bias products, and $\delta\boldsymbol{X}^s_{\text{igs}}$, $\delta dt^s_{\text{igs,IF}}$ and $\delta B^s_{\text{igs,IF}}$ are the corresponding product errors, respectively. After these SSR products are applied, product errors propagate into the observation model, and (1) can be rewritten:

$$\begin{cases} \overline{P}^s_{r,\text{IF}} = \overline{\rho}^s_r + c(t_{r,\text{IF}} - t^s_{\text{igs,IF}}) + m^s_h w_r \\ \qquad\qquad + (\boldsymbol{u}^s_r\delta\boldsymbol{X}^s_{\text{igs}} - \delta t^s_{\text{igs,IF}}) + e^s_{\text{IF}} \\ \overline{L}^s_{r,\text{IF}} = \overline{\rho}^s_r + c(t_{r,\text{IF}} - t^s_{\text{igs,IF}}) + m^s_h w_r + \lambda_{IF}\tilde{N}^s_{r,\text{IF}} \\ \qquad\qquad + (\boldsymbol{u}^s_r\delta\boldsymbol{X}^s_{\text{igs}} - \delta t^s_{\text{igs,IF}} - \lambda_{\text{IF}}B^s_{\text{igs,IF}}) + \varepsilon^s_{\text{IF}} \end{cases} \tag{6}$$

where $\overline{P}$ and $\overline{L}$ are the corrected code and carrier-phase measurements using the OSB products; $\overline{\rho}^s_r$ denotes the geometric distance between the receiver and satellite antenna phase centers calculated using orbit products; $\boldsymbol{u}^s_r\delta\boldsymbol{X}^s_{\text{igs}}$ is the line-of-sight projection of orbit product errors, and $\boldsymbol{u}^s_r$ is the unit vector from the satellite s to the receiver r. Due to the much higher noise levels of code measurements (decimeter-level) compared to carrier-phase observations (Gao et al., 2024), code measurements are assigned low weights in the estimation, and the solution is predominantly determined by the more precise carrier-phase measurements.

PPP processing is typically performed using a filtering-based approach, in which ambiguity parameters are estimated as one constant for each arc, with its variances propagated between epochs. Under float ambiguity conditions, the SSR product errors are effectively decomposed into two components. The stable or slowly varying components are absorbed by the highly correlated ambiguity parameters (Lou et al., 2014; Tian et al., 2025), while time-varying or abrupt errors primarily retain in the ambiguity-float phase residuals. Although small common errors may also be partially absorbed by the receiver clock and zenith tropospheric delay parameters, their magnitudes are small and therefore neglected here for clarity. Accordingly, the PPP observation model can be reformulated as:

$$\begin{cases} \overline{P}^s_{r,\text{IF}} = \overline{\rho}^s_r + c(\widehat{t}_{r,\text{IF}} - t^s_{\text{igs,IF}}) + m^s_h\hat{w}_r \\ \qquad\qquad + [(\boldsymbol{u}^s_r\delta\boldsymbol{X}^s_{\text{igs}} - \delta t^s_{\text{igs,IF}}) + e^s_{e,\text{IF}}] \\ \overline{L}^s_{r,\text{IF}} = \overline{\rho}^s_r + c(\widehat{t}_{r,\text{IF}} - t^s_{\text{igs,IF}}) + m^s_h\hat{w}_r \\ \qquad\qquad + \lambda_{\text{IF}}\hat{N}^s_{r,\text{IF}} + [\delta\ddot{\eta}^s_{r,\text{LOS}} + \varepsilon^s_{\text{IF}}] \end{cases} \tag{7}$$

with

$$\begin{cases} t_{r,\text{IF}} = t_r + b_{r,\text{IF}}/c \\ \hat{N}^s_{r,\text{IF}} = N^s_{r,\text{IF}} + B_{r,\text{IF}} - b_{r,\text{IF}}/\lambda_{\text{IF}} + \delta\eta^s_{r,\text{absd}}/\lambda_{\text{IF}} \end{cases} \tag{8}$$

where $\widehat{t}_{r,\text{IF}}$, $\hat{w}_r$ and $\hat{N}^s_{r,\text{IF}}$ are the estimated values of the corresponding parameters. Because satellite orbit, clock, and phase bias products are mutually correlated, their error effects cannot be completely separated and are therefore treated as a combined error term $\delta\eta^s_{r,\text{LOS}} = \boldsymbol{u}^s_r\delta\boldsymbol{X}^s_{\text{igs}} - \delta t^s_{\text{igs,IF}} - \lambda_{\text{IF}}\delta B^s_{\text{igs,IF}}$. $\delta\eta^s_{r,\text{absd}}$ denotes the component of this combined error term absorbed by the ambiguity parameters ($\hat{N}^s_{r,\text{IF}}$), $\delta\ddot{\eta}^s_{r,\text{LOS}}$ represents the residual component remaining in the ambiguity-float phase residuals, and $\delta\eta^s_{r,\text{absd}} + \delta\ddot{\eta}^s_{r,\text{LOS}} = \delta\eta^s_{r,\text{LOS}}$. To ensure the robustness of the estimation, the Detection, Identification, and Adaptation (DIA) algorithm (Baarda, 1968; Teunissen, 2018) is applied to detect and mitigate the gross errors in the observations in the PPP filtering process. This prevents individual anomalous observations from contaminating the parameter estimates.

As shown in (7), combined SSR product errors are distributed across ambiguity estimates and phase residuals in the float solution. Before ambiguities are fixed, phase residuals may not fully reflect the combined SSR product errors, as a portion of the errors is absorbed by the ambiguity parameters. Only after ambiguities are fixed to their integer values do the absorbed errors become released into the residuals, enabling complete error detection. This is why existing SSR product monitoring methods typically employ ambiguity-fixed phase residuals, which allow combined product errors to be fully revealed through the phase residuals. However, this approach is only applicable to ambiguity-fixed SSR products and cannot reliably evaluate ambiguity-float SSR products. As a result, the error magnitude of ambiguity-float SSR products cannot be accurately quantified, making them difficult to use effectively. To address this limitation, the proposed method extracts both error components (float ambiguity deviations and ambiguity-float phase residuals) and jointly considers them to enable a comprehensive quality assessment for both ambiguity-fixed and ambiguity-float SSR products.

The ambiguity-float phase residuals are obtained by differencing the IF carrier-phase measurements and the sum of the computed geometric range and other estimated parameters:

$$\begin{aligned} \phi^s_{L_{r,\text{IF}}} &= \overline{L}^s_{r,\text{IF}} - \left\{\overline{\rho}^s_r + c(\widehat{t}_{r,\text{IF}} - t^s_{\text{igs,IF}}) + m^s_h\hat{w}_r + \lambda_{\text{IF}}\hat{N}^s_{r,\text{IF}}\right\} \\ &= \delta\ddot{\eta}^s_{r,\text{LOS}} + \varepsilon^s_{\text{IF}} \end{aligned} \tag{9}$$

The derived phase residuals $\phi^s_{L_{r,\text{IF}}}$ primarily consist of the portion of the combined SSR product errors that

is not absorbed by the ambiguity parameters, together with measurement noise. In practice, station-specific environmental effects may introduce abnormal residuals that are unrelated to SSR product errors. The identification and removal of such outliers are described in the following sections.

For the errors absorbed by the float ambiguity parameters, it can be seen from (8) that a float ambiguity consists of three parts: the true integer value, the receiver hardware delay, and the absorbed component of the combined SSR product error. After removing the receiver hardware delay, the deviation of the float ambiguity from its true integer value represents the absorbed combined SSR product error. Based on this decomposition, a procedure can be employed to separate and resolve the float ambiguities.

Since the IF ambiguities are non-integer, they can be further separated into Wide-Lane (WL) and Narrow-Lane (NL) components:

$$\begin{aligned}\lambda_{\mathrm{IF}}\hat{N}^s_{r,\mathrm{IF}} = {} & \frac{cf_j}{f_i^2 - f_j^2}N^s_{r,\mathrm{wl}} + \frac{c}{f_i + f_j}N^s_{r,\mathrm{nl}} \\ & + \lambda_{\mathrm{IF}}B_{r,\mathrm{IF}} - b_{r,\mathrm{IF}} + \delta\eta^s_{r,\mathrm{absd}}\end{aligned} \tag{10}$$

where $N^s_{r,\mathrm{wl}}$ and $N^s_{r,\mathrm{nl}}$ are the WL and NL integer ambiguities, respectively. The WL ambiguities can be derived from the Hatch-Melbourne-Wübbena (HMW) combination (Hatch, 1983; Melbourne, 1985; Wübbena, 1985):

$$\tilde{N}^s_{r,\mathrm{wl}} = \left(\frac{L^s_{r,i}}{\lambda_i} - \frac{L^s_{r,j}}{\lambda_j} - \frac{f_iP^s_{r,i} + f_jP^s_{r,j}}{(f_i + f_j)\lambda_{\mathrm{wl}}}\right) = N^s_{r,\mathrm{wl}} + d_{r,\mathrm{wl}} - d^s_{\mathrm{wl}} \tag{11}$$

where $d_{r,\mathrm{wl}}$ and d^s_{wl} are the WL Fractional-Cycle-Biases (FCBs) of the receiver and satellite, respectively. The satellite WL FCBs are corrected using the WL FCB products, and the receiver WL FCBs are eliminated by satellite-differencing. The WL FCB products are derived from code and phase OSB products through an MW combination. After eliminating these biases, the WL ambiguities can usually be fixed accurately with high success rate (Du et al., 2022). The satellites whose WL ambiguities cannot be fixed are excluded from processing at the affected stations. If WL fixing fails at more than half of the monitoring stations for a particular satellite, the corresponding SSR products are flagged as unreliable. For satellites with fixed WL ambiguities, the Satellite-Differenced (SD) NL float ambiguities are expressed as (Ge et al., 2008):

$$\begin{aligned}\Delta\tilde{N}^{p,q}_{r,\mathrm{nl}} &= \frac{(f_i + f_j)}{c}\lambda_{\mathrm{IF}}\Delta\hat{N}^{p,q}_{r,\mathrm{IF}} - \frac{f_j}{f_i - f_j}\Delta N^{p,q}_{r,\mathrm{wl}} \\ &= \Delta N^{p,q}_{r,\mathrm{nl}} + \frac{(f_i + f_j)}{c}\Delta(\delta\eta^{p,q}_{r,\mathrm{absd}})\end{aligned} \tag{12}$$

where p is the reference satellite, and q is a non-reference satellite. The reference satellite is selected from the common-view satellites within a monitoring network. At the first epoch, the satellite with the highest elevation is chosen as the reference and maintained continuously across epochs if its elevation remains above 20°. Consequently, the SD NL ambiguity deviations are expressed as:

$$\delta(\Delta N^{p,q}_{r,\mathrm{nl}}) = \Delta\tilde{N}^{p,q}_{r,\mathrm{nl}} - \Delta N^{p,q}_{r,\mathrm{nl}} = \frac{f_i + f_j}{c}\Delta(\delta\eta^{p,q}_{r,\mathrm{absd}}) \tag{13}$$

where $\delta(\Delta N^{p,q}_{r,\mathrm{nl}})$ represents the portion of SD combined SSR product error absorbed by the ambiguity. It is the cumulative effect of errors from satellite orbit, clock, and phase bias products.

Quality monitoring and error correction

After extracting the SD NL ambiguity deviations and the ambiguity-float phase residuals at all monitoring stations, quality monitoring and error correction are performed through a two-step strategy. First, multi-station consistency validation is applied to identify and remove outliers caused by local environmental effects or abnormal observations. This step ensures that the retained values reliably reflect the combined SSR product errors. Second, the validated SD NL ambiguity deviations and the ambiguity-float phase residuals are used to derive corrections for mitigating product errors and to assess the quality of the corrected SSR products.

Multi-station consistency validation and outlier detection

For a given satellite, the combined SSR product error represents the cumulative effect of errors in orbit, clock, and phase bias products. Although orbit errors are direction-dependent, previous studies have demonstrated that their impact on PPP solutions still contains significant common-mode components within regional networks with a radius of approximately 700 km (Lou et al., 2014). The extracted SD NL ambiguity deviations and the ambiguity-float phase residuals should therefore exhibit interstation consistency. However, individual stations can be affected by measurement noise or unmodeled local effects. Separate outlier detection is therefore applied to the ambiguity deviations and the ambiguity-float phase

residuals to remove contaminated values before further analysis.

Before outlier detection, the SD NL ambiguity deviations and the ambiguity-float phase residuals are excluded from analysis if the standard deviation of the ambiguity estimate exceeds one centimeter (Laurichesse et al., 2009), or if the change in the NL ambiguity deviation exceeds 0.05 cycles over 10 epochs. This preliminary screening removes data from the convergence period. Subsequently, a two-step outlier detection procedure is applied independently to the ambiguity deviations and the ambiguity-float phase residuals. The first step uses the Interquartile Range (IQR) method to remove extreme values based on the overall statistical distribution. The second step employs the Density-Based Spatial Clustering of Applications with Noise (DBSCAN) algorithm to identify locally isolated anomalies. By removing global extreme values and then identifying local density anomalies, this approach ensures a cleaner dataset for subsequent SSR product correction and quality assessment.

The IQR method is a classical statistical method that detects outliers based on the distribution of data between the first and third quartiles (Rousseeuw & Hubert, 2018). The IQR-based boundaries are defined as:

$$\begin{cases} \xi_{\text{upper}} = Q_3 + k \times (Q_3 - Q_1) \\ \xi_{\text{lower}} = Q_1 - k \times (Q_3 - Q_1) \end{cases} \tag{14}$$

where Q_1 and Q_3 denote the first and third quartiles of the inputted data, respectively; ξ_{lower} and ξ_{upper} are calculated as lower and upper bounds; k determines the filter strictness, and is set to 1.5 in this study following Vinutha et al. (2018).

The candidate SD NL ambiguity deviations and the ambiguity-float phase residuals that pass the IQR filtering may still contain residual local noise. The DBSCAN algorithm (Ester et al., 1996) is applied to further identify locally isolated anomalies. Compared with the traditional clustering algorithms such as K-means or hierarchical clustering, DBSCAN does not predefine the number of clusters and can identify clusters with arbitrary shapes. Its strong robustness to noise makes it particularly suitable for complex datasets with outliers (Khan et al., 2014). In this study, the DBSCAN is applied separately to the SD NL ambiguity deviations and the ambiguity-float phase residuals of each satellite, collected at all monitoring stations at each epoch.

$$N_{\text{Eps}}(m) = \{n \in D | d(m,n) \leq e\} \tag{15}$$

with

$$D = \{\delta(\Delta N_{1,\text{nl}}^{p,q}), \delta(\Delta N_{2,\text{nl}}^{p,q}), \ldots, \delta(\Delta N_{r,\text{nl}}^{p,q})\} \tag{16}$$

where D denotes the database of objects; m is an arbitrary combined product error in the set, and n is the candidate to be evaluated; $d(m,n)$ represents the absolute difference, and Eps is a virtual region centered at m with a radius of e. In this study, the radius is set to 0.05 cycles for SD NL ambiguity deviations and one centimeter for phase residuals.

DBSCAN identifies a core point as one that has at least the minimum number of neighboring points (M_{pts}) within the radius of e.

$$N_{\text{Eps}}(m) > M_{\text{pts}} \tag{17}$$

where M_{pts} is set to four in this study. Clusters are then formed by grouping all points that are density-reachable from these core points, as illustrated to demonstrate the principle in Fig. 2. If two core points fall within neighborhoods of each other, they are assigned to the same cluster. The points within the neighborhood of a core point but not core points are labeled as border points and included in the cluster, while those that are neither core nor border are classified as noise and considered outliers. If the SD NL ambiguity deviations or the phase residuals of a satellite fail to form a cluster, or if multiple inconsistent clusters are detected, the combined SSR product of that satellite is considered anomalous, and an alarm flag is assigned.

Correction computation and reliability assessment

After removing the outliers, the SD NL ambiguity deviations and the ambiguity-float phase residuals are treated differently according to their statistical characteristics. Due to their temporal stability, the SD NL ambiguity deviations are used to estimate the corrections that mitigate systematic and regionally consistent errors in the original SSR

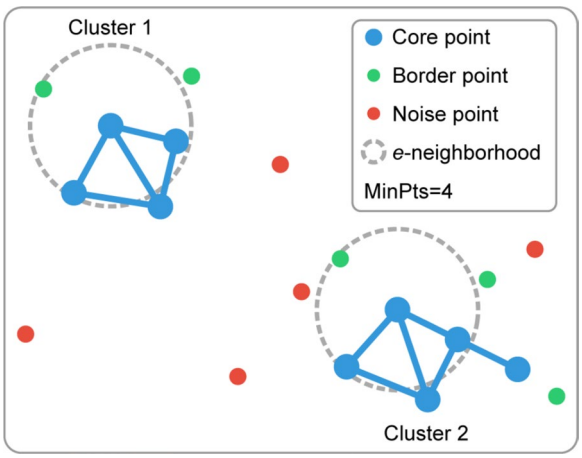

Fig. 2 Illustration of DBSCAN clustering showing core points (blue), border points (green), and noise points (red). MinPts represents the minimum number of neighboring points

products. In contrast, the phase residuals mainly reflect the remaining errors after correction, which are more sensitive to observation noise, are used to assess the quality of the corrected products and to detect significant anomalies. This section first describes the correction estimation and then presents the quality assessment of the corrected SSR products.

The correction value of the combined SSR product error is derived by computing a weighted average of the SD NL ambiguity deviations obtained at all monitoring stations:

$$\Delta C^{p,q}_{\mathrm{SSR,nl}} = -\overline{\delta(\Delta N^{p,q}_{\mathrm{nl}})} = -\frac{\sum_{r=1}^{n} w_r^{p,q}\,\delta(\Delta N^{p,q}_{r,\mathrm{nl}})}{\sum_{r=1}^{n} w_r^{p,q}} \tag{18}$$

where $w_r^{p,q}$ is the weight for station r, which is calculated as the inverse of the variance of the SD NL ambiguity deviation. The resulting weighted average $\overline{\delta(\Delta N^{p,q}_{\mathrm{nl}})}$ represents the portion of SD combined SSR product error absorbed by ambiguity. It also serves as the correction value ($\Delta C^{p,q}_{\mathrm{SSR,nl}}$) used to mitigate systematic and regionally consistent errors in the original SSR products.

The reliability of estimated correction is assessed through the weighted standard deviation of the input values with respect to $\overline{\delta(\Delta N^{p,q}_{\mathrm{nl}})}$

$$\Delta\sigma^{p,q}_{\mathrm{corr}} = \sqrt{\frac{\sum_{i=1}^{n} w_r^{p,q}\left[\delta(\Delta N^{p,q}_{r,\mathrm{nl}}) - \overline{\delta(\Delta N^{p,q}_{\mathrm{nl}})}\right]^2}{\sum_{i=1}^{n} w_r^{p,q}}} \tag{19}$$

where $\Delta\sigma^{p,q}_{\mathrm{corr}}$ quantifies the inter-station consistency of the input values used for calculating correction. A smaller $\Delta\sigma^{p,q}_{\mathrm{corr}}$ indicates higher consistency among stations and implies that a larger portion of the common SSR product error can be mitigated. If $\Delta\sigma^{p,q}_{\mathrm{corr}}$ exceeds a predefined threshold of 0.1 cycles in our implementation, the combined SSR product is considered unreliable and is flagged accordingly. Otherwise, the correction value and its associated reliability metric are retained.

In practical applications, the SD corrections are converted to undifferenced corrections by imposing a zero-sum constraint across all satellites:

$$\begin{bmatrix} \boldsymbol{D} \\ \boldsymbol{e}^{\mathrm{T}} \end{bmatrix} \boldsymbol{C}_{\mathrm{SSR,nl}} = \begin{bmatrix} \Delta\boldsymbol{C}_{\mathrm{SSR,nl}} \\ 0 \end{bmatrix} \tag{20}$$

where $\Delta\boldsymbol{C}_{\mathrm{SSR,nl}} = [\Delta C^{p,1}_{\mathrm{SSR,nl}}, \Delta C^{p,2}_{\mathrm{SSR,nl}}, \ldots, \Delta C^{p,s}_{\mathrm{SSR,nl}}]^{\mathrm{T}}_{(s-1)\times 1}$ is the vector of the SD corrections relative to the reference satellite p, and $\boldsymbol{C}_{\mathrm{SSR,nl}} = [C^{1}_{\mathrm{SSR,nl}}, C^{2}_{\mathrm{SSR,nl}}, \cdots, C^{s}_{\mathrm{SSR,nl}}]^{\mathrm{T}}_{s\times 1}$ is the vector of undifferenced corrections to be estimated; $\boldsymbol{D}$ is a $(s-1)\times s$ differencing matrix in which each row corresponds to one SD correction (1 for the target satellite, -1 for the reference satellite, and 0 elsewhere); $\boldsymbol{e}^{\mathrm{T}} = [1,\ 1, \ldots,\ 1]_{s\times 1}$ is the constraint vector. The resulting undifferenced corrections ($C^{s}_{\mathrm{SSR,nl}}$) include a common offset. To ensure temporal continuity of this common offset, a reference alignment procedure (Banville et al., 2020) is applied when converting the SD corrections to undifferenced corrections. In positioning, this offset is absorbed by the ambiguities and the receiver clock, therefore does not affect positioning accuracy. The reliability indicators ($\sigma^{s}_{\mathrm{corr}}$) of the undifferenced corrections are propagated from the SD domain according to the law of error propagation. Finally, the corrections ($C^{s}_{\mathrm{SSR,nl}}$) can be expressed in the OSB format for each individual frequency as $C^{s}_{\mathrm{SSR},i}$ and $C^{s}_{\mathrm{SSR},j}$ following Shu et al. (2024), so that they can be directly applied to the measurements together with the SSR products.

After applying the estimated corrections, the remaining errors of the corrected SSR products are mainly manifested in the ambiguity-float phase residuals at the monitoring stations. Therefore, the ambiguity-float phase residuals are adopted as the primary indicator for assessing the quality of the corrected SSR products. For each satellite, the phase residual-based quality metric is defined as:

$$\overline{\phi^{s}_{L_{\mathrm{IF}}}} = \frac{\sum_{r=1}^{n} w_r^{s}\phi^{s}_{L_{\mathrm{r,IF}}}}{\sum_{r=1}^{n} w_r^{s}} \tag{21}$$

where $\overline{\phi^{s}_{L_{\mathrm{IF}}}}$ denotes the weighted mean of the ambiguity-float phase residuals for all monitoring stations, and the station weight w_r^{s} is given by the inverse of the corresponding phase residual variance. In addition, the inter-station consistency of the ambiguity-float phase residuals is quantified using the consistency metric σ^{s}_{ϕ}, which is computed following the method described in Eq. (19).

Although the ambiguity-float phase residuals constitute the principal quality indicator, the consistency information derived from both the ambiguity-float phase residuals and the NL ambiguity deviations is also used as an auxiliary reliability check. These consistency measures are separately used to verify the reliability of the computed mean ambiguity-float phase residuals and the applied corrections, thereby reliably assessing the quality of the corrected SSR products. The final quality metric of the SSR products is therefore defined as (Li et al., 2024; Wang & Shen, 2020; Wang et al., 2015):

$$\sigma^{s}_{\mathrm{SSR}} = (\overline{\phi^{s}_{L_{\mathrm{IF}}}} + K\sigma^{s}_{\phi} + K\sigma^{s}_{\mathrm{corr}})/K \tag{22}$$

where K is the Gaussian quantile corresponding to the integrity risk P, defined as $K = f^{-1}(1-P)$, where $f^{-1}(\cdot)$

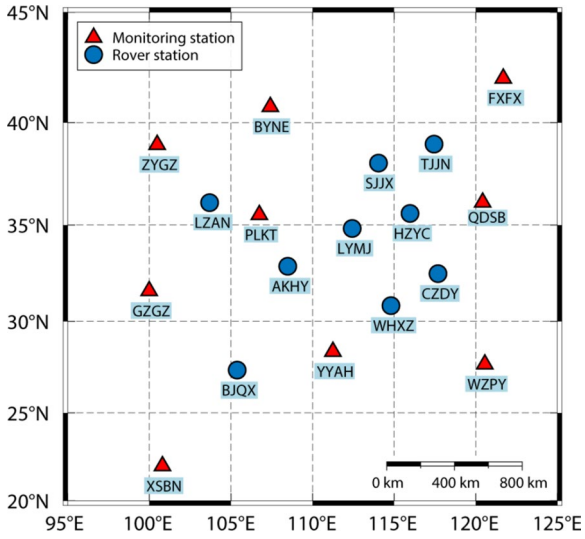

Fig. 3 Distribution of the stations in the study. Red triangles and blue points are the monitoring and rover stations, respectively

denotes the inverse cumulative distribution function of the standard normal distribution (Wang et al., 2015). In this study, P is set to 2×10^{-2}/h, resulting in $K = 2.33$, following Li et al. (2024). Finally, the estimated corrections $(C^s_{\mathrm{SSR},i}, C^s_{\mathrm{SSR},j})$ for the combined SSR product of each satellite, together with the quality indicators $(\sigma^s_{\mathrm{SSR}})$ of corrected SSR products, are provided to users, thereby enabling reliable PPP-AR positioning.

Application of monitoring products

The monitoring outputs are incorporated in user processing to enhance positioning performance. For each satellite s, the correction values $(C^s_{\mathrm{SSR},i}, C^s_{\mathrm{SSR},j})$ are applied to the original observations together with the original SSR products. To properly weight the corrected measurements in the filter, their variance is calculated as the sum of the carrier-phase observation variance and the product variance, assuming the two are independent:

$$\sigma^2 = \sigma_0^2 + \sigma^2_{\mathrm{SSR}} \tag{23}$$

where σ_0^2 denotes the carrier-phase observation variance, and σ^s_{SSR} represents the variance of the products. In addition, the SSR products flagged as unreliable are excluded from the positioning to prevent degraded solutions caused by anomalous products:

Data description and processing strategy

GNSS data from Day-of-Year (DOY) 001–031 of 2022 were collected at a 30 s sampling interval. As shown in Fig. 3, nine stations (marked with red triangles) were selected as monitoring stations to continuously evaluate the quality of real-time SSR products. These stations are sparsely distributed across more than 20 provinces in China, covering an area of approximately $2000 \times 1600\ \mathrm{km}^2$. Another nine stations (marked with blue points) were selected as rovers for kinematic PPP-AR positioning. Real-time orbit, clock, and code/phase bias corrections for GPS and Galileo satellites were obtained from the CNES real-time product archive to avoid potential delays in real-time data transmission.

Table 1 summarizes the processing strategies used in this study. After fixing the WL ambiguities, float NL ambiguities are obtained. The proposed method, Float-Ambiguity Deviation and Phase Residual-based Quality Monitoring and Correction (FAP-QMC), performs the quality monitoring and error correction of SSR products using both the float ambiguity deviations and the

Table 1 Processing strategies for server-side monitoring and user-side positioning

Item	Strategy
Station coordinate	Server: Fixed User: Estimated in the epoch-wise kinematic mode
Observations	IF combinations, GPS L1 + L2, Galileo E1 + E5a
Phase ambiguities	Constant for each arc Server: WL fixed, NL float User: WL & NL both fixed
Raw observation noise and weight	Code 30 cm, phase 3 mm Elevation-dependent, $\sin(E)$
Satellite orbit/clock	Fixed with RT orbit/clock from CNES
Code and phase bias	Fixed with RT OSB from CNES
Phase windup effect	Corrected
Estimator	Forward Kalman filter
Tropospheric wet delay	$10^{-4}\ \mathrm{m} \cdot \mathrm{s}^{-1/2}$ random walk process with a priori variance of $0.15^2\ \mathrm{m}^2$ (Shu et al., 2021)
Receiver clock	Epoch-wise estimated for each system

ambiguity-float phase residuals. For comparison, two additional methods are considered: (1) Phase Residual-based Quality Monitoring (PR-QM), which utilizes ambiguity-fixed phase residuals (i.e., observed-minus-computed phase values from Eq. 9) as quality indicators. The aggregated results of these quality indicators at multiple monitoring stations are then used to adjust satellite weight in the filter as described in Li et al. (2024); (2) No Quality Monitoring (NO-QM), in which PPP-AR users directly use the unmonitored SSR products. The performance of all three methods is analyzed in both the PPP-float and PPP-AR stages. In all cases, the same CNES orbit, clock, and OSB products are used, and positioning performance is evaluated using the data at the nine rover stations.

Results and analysis

To evaluate the effectiveness of the proposed FAP-QMC method, this section presents comprehensive experimental analysis in two parts. First, the characteristics of float ambiguity deviations and ambiguity-float phase residuals are analyzed to verify their suitability for quality monitoring and error correction of SSR products. Second, the performance of FAP-QMC is compared with two baseline methods (PR-QM and NO-QM) at both the float PPP and PPP-AR stages, with the metrics: positioning accuracy, outlier mitigation, fixing rate, incorrect fixing rate, and time-to-first-fix.

Analysis of float ambiguity deviations and phase residuals

This section presents an experimental analysis to verify the theoretical foundation of the proposed method. Specifically, we investigate how combined SSR product errors manifest in float ambiguity deviations and ambiguity-float phase residuals and demonstrate the feasibility of deriving corrections from the ambiguity deviations.

Reliable monitoring and correction of SSR product errors require a clear understanding of how different error types are distributed between the ambiguity deviations and the ambiguity-float phase residuals. As established in the methodology section, the sum of float ambiguity deviations and ambiguity-float phase residuals is theoretically equivalent to the ambiguity-fixed phase residuals under identical observation models and estimation settings. To verify this relationship and demonstrate the complementary roles of these two quantities, Fig. 4 presents the time series of SD NL ambiguity deviations and ambiguity-float phase residuals for multiple satellites at station LZAN. Three typical error patterns commonly found in SSR products are intentionally introduced after ambiguity convergence: a constant offset of 3 cm, a linear ramp error at 0.2 ns per hour, and step errors of 5 cm occurring every 10 min. These controlled errors allow us to clearly observe how each quantity responds to different error characteristics.

The results reveal distinct sensitivities to different error patterns. Constant errors are almost entirely absorbed by float ambiguity estimates, with negligible impact on ambiguity-float phase residuals. For ramp errors, a part of the errors is absorbed by the ambiguity estimates, while the remaining component appears in ambiguity-float phase residuals. Step errors are primarily reflected in the ambiguity-float phase residuals, with limited absorption by ambiguities. The above observations demonstrate that ambiguity deviations primarily capture temporally stable SSR product errors, whereas the ambiguity-float phase residuals are more sensitive to time-varying and step errors. After ambiguity convergence, the sum of ambiguity deviations and ambiguity-float phase residuals closely matches the ambiguity-fixed phase residuals, with differences approaching zero. This confirms the theoretical consistency between the proposed monitoring strategy and conventional ambiguity-fixed phase residual-based approaches. The two quantities therefore play complementary roles in SSR product quality characterization. Note that during the convergence period, PPP solutions are unreliable. Strict quality control procedures (detailed in the methodology section) are therefore applied in all subsequent analyses to eliminate effects related to convergence.

Building on the verified equivalence between the combined float quantities and ambiguity-fixed phase residuals, an important advantage of the proposed method is its applicability to the products with ambiguities not fixed. For error types such as the constant and ramp errors shown in Fig. 4, ambiguities cannot be fixed once the accumulated error exceeds a tolerable level, rendering monitoring of traditional ambiguity-fixed phase residual ineffective. By jointly considering float ambiguity deviations and ambiguity-float phase residuals, the monitoring capability to these scenarios can be effectively extended. Additionally, the ambiguity deviations exhibit strong temporal stability, making them well-suited for modeling and generating corrections to mitigate combined SSR product errors. The ambiguity-float phase residuals, which are more affected by measurement noise, are better suited for evaluating residual errors after correction.

The corrections derived from ambiguity deviations are intended to mitigate the common-mode components of the combined SSR product errors observed across the monitoring network. Figure 5 illustrates the SD NL ambiguity deviations (computed using Eq. 12) for a subset of satellites on DOY 025, 2022 under normal service-side monitoring conditions. The black dashed lines denote the weighted mean of deviations used to generate corrections. A strict quality control procedure (detailed in

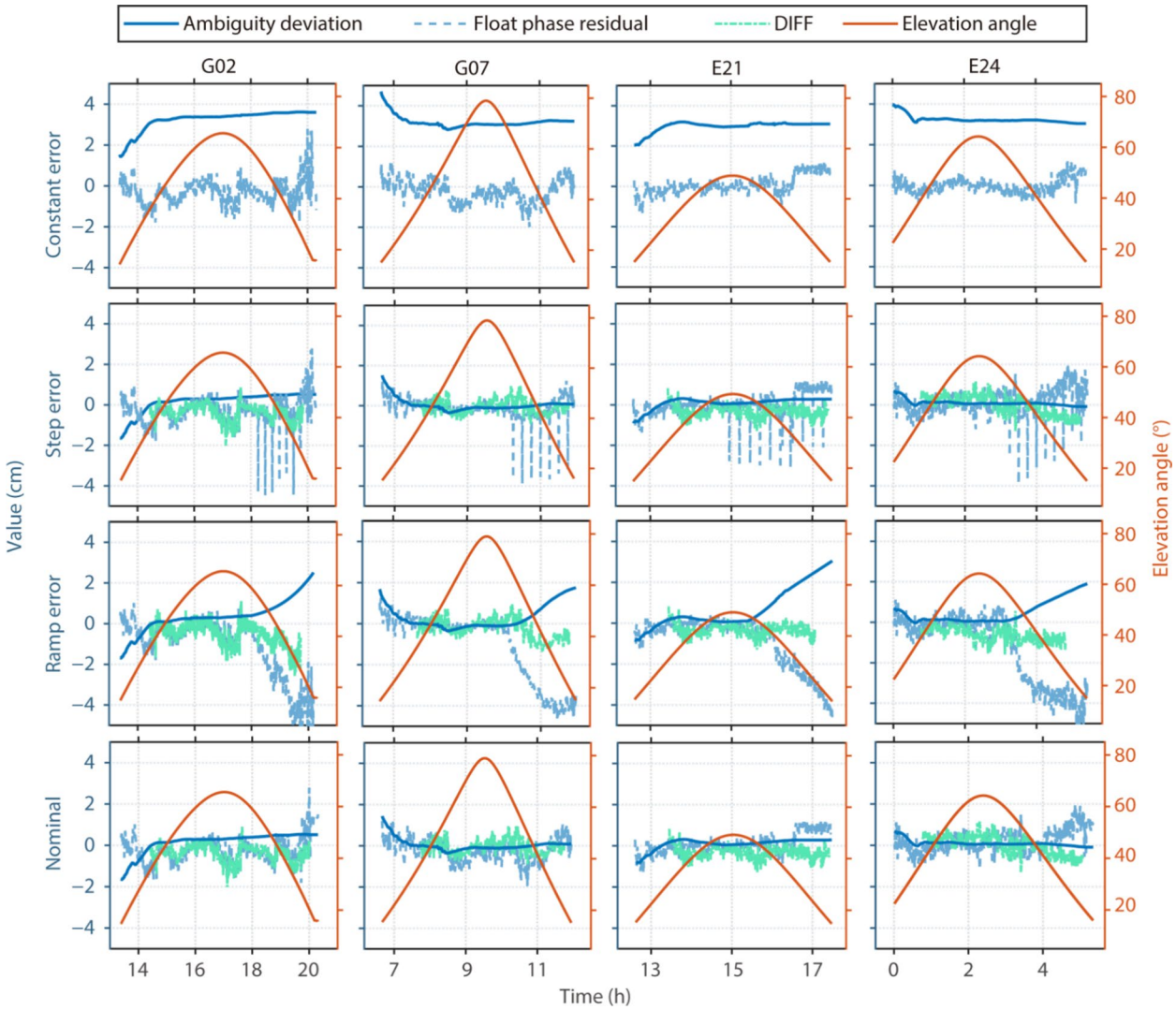

Fig. 4 Time series of SD NL float ambiguity deviations and ambiguity-float phase residuals at station LZAN. Columns show different satellites; rows show SSR product error patterns (top to bottom: constant, step, ramp, no error) introduced after ambiguity convergence. DIFF quantifies the difference between the combined float quantities and the ambiguity-fixed phase residuals

the methodology section) was applied to remove outliers caused by local observation environments, ensuring that only screened NL ambiguity deviations were used for deriving corrections. To evaluate the inter-station consistency of these deviations, the Weighted Standard Deviation (WSTD) at each station relative to the weighted mean was calculated with Eq. (19). The results show a maximum WSTD of 0.04 cycles for satellite E13 and a mean WSTD across all satellites within 0.03 cycles, indicating high consistency across the monitoring network. This high inter-station consistency suggests that the float ambiguity deviations are primarily driven by the common SSR product errors rather than local noise, supporting their use for generating corrections to mitigate regionally consistent SSR product errors.

Notably, significant ambiguity offsets are observed for satellites such as G06 and E03, which prevent ambiguity fixing. In the traditional monitoring methods based on ambiguity-fixed phase residuals, such SSR products may not be applied due to their uncertain quality. However, the spatially consistent ambiguity deviations observed here represent common-mode product errors. The proposed method does not reject these products. Instead, it utilizes these stable and spatially consistent float ambiguity deviations to mitigate SSR product errors, while ambiguity-float phase residuals are used to evaluate

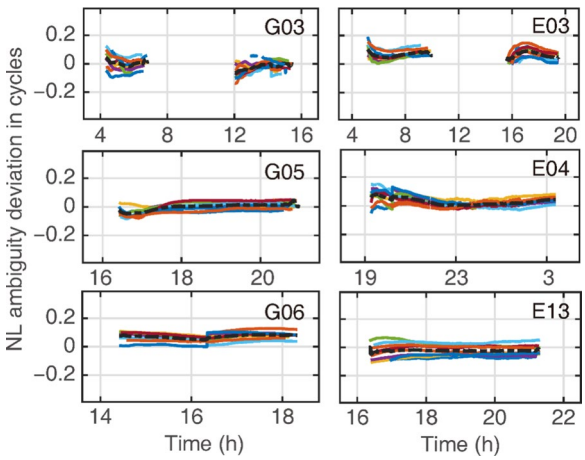

Fig. 5 SD NL ambiguity deviations at monitoring stations on DOY 025, 2022, with satellite orbit, clock, and phase OSB products applied. The black dashed lines denote the weighted mean deviations used for correction generation, whereas each color indicates a different monitoring station

the remaining uncorrected errors. This strategy allows potentially valuable SSR products to be retained and properly assessed, enabling previously excluded products to be converted into reliable ones and improving the robustness and availability of PPP-AR solutions.

When precise SSR products are applied, the SD NL float ambiguities are expected to approach integer values. To assess the effectiveness of the derived corrections, Fig. 6 illustrates the distribution of the SD NL ambiguity deviations across all rover stations over one month, using SSR products processed by three monitoring strategies: FAP-QMC, PR-QM, and NO-QM. Applying the derived corrections together with the original SSR products (orbits, clocks, and OSBs) effectively reduces the SD NL ambiguity deviations, making them closer to integer values as expressed in (12). Although all methods exhibit bell-shaped distributions, clear differences can be observed. The distribution obtained using the proposed FAP-QMC method is narrower and more concentrated. Approximately 90% of the deviations fall within ± 0.25 cycles, and 76.3% (GPS) and 75.2% (Galileo) lie within ± 0.15 cycles, corresponding to improvements of 7.9% and 13.2%, relative to PR-QM, respectively. These results confirm that the proposed FAP-QMC method effectively enhances the quality of service-side SSR products and provides a more reliable foundation for subsequent PPP-AR positioning.

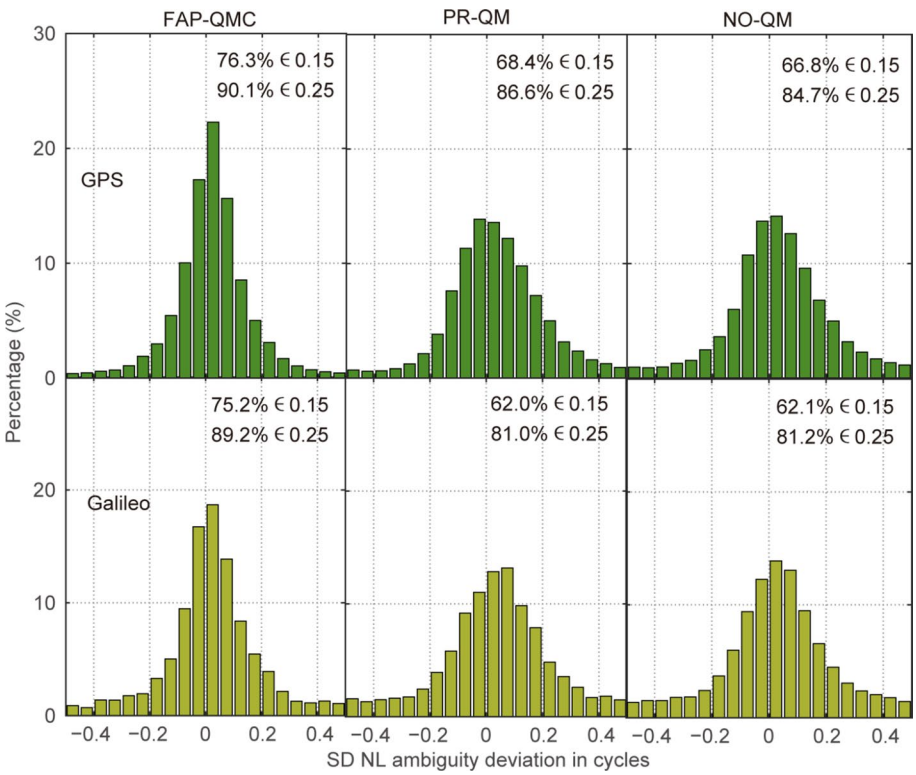

Fig. 6 Histograms of SD NL ambiguity deviations for GPS (top) and Galileo (bottom) using different product monitoring methods: FAP-QMC (left column), PR-QM (central column), and NO-QM (right column) during the period from DOY 001 to 031 in 2022

Validation in ambiguity-float solution

Reliable estimation of float ambiguities is essential for successful PPP-AR, as it provides the foundation for subsequent integer ambiguity resolution. To evaluate performance of the proposed method at the ambiguity-float solution stage, the data collected from all rover stations over DOY 001–031, 2022, were processed with the FAP-QMC, PR-QM, and NO-QM methods.

Figure 7 presents the positioning error series for station CZDY over one month using three monitoring strategies. Brief gaps are visible due to interruptions in real-time observation data collection. With the NO-QM method, significant positioning anomalies are observed on DOY 028 and DOY 031, whereas both FAP-QMC and PR-QM methods produce stable results. To investigate the cause of these anomalies, a detailed analysis of DOY 028 is presented in Fig. 8. The left panel shows the positioning details, while the right panel presents the corresponding SSR product quality assessment. Specifically, the Signal-in-Space Range Errors (SISREs) were computed by comparing CNES real-time orbit and clock products with final products from the Center for Orbit Determination in Europe (CODE) (Montenbruck et al., 2018; Zhang et al., 2019). Furthermore, the phase OSBs were converted into WL and NL FCBs (Laurichesse, 2012). The analysis reveals that satellites E07 and E33 exhibited abrupt jumps in NL FCB during the period of approximately 11:30–12:00 and 15:20–17:20 (GPST), although their orbit and clock products were normal. Both PR-QM and the proposed FAP-QMC method successfully detected and excluded these anomalous SSR products, thereby avoiding their adverse impact on positioning. Notably, the proposed FAP-QMC method achieves smoother positioning results compared to PR-QM. A similar issue occurred on DOY 031 with satellite G09, whose sudden NL FCB jump caused the observed fluctuations with the NO-QM method.

Figure 9 summarizes the Three-Dimensional (3D) positioning Root Mean Square Error (RMSE) for all rover stations. The proposed FAP-QMC method achieves an average RMSE of 5.6 cm, outperforming PR-QM (6.1 cm) and NO-QM (8.2 cm). However, this overall statistic does not fully reflect the capability of the proposed method in mitigating positioning errors, as the periods of degraded positioning are masked in the long time series and thus diluted in the overall RMSE. To illustrate method performance during these challenging periods, representative positioning deviations are presented in Fig. 10. The results show that FAP-QMC maintains more stable performance. Furthermore, when calculating RMSE for the epochs surrounding these periods (2 h before and after), the 3D RMSE values are 6.4 cm for FAP-QMC, 7.6 cm for PR-QM, and 13.7 cm for NO-QM. These results demonstrate that FAP-QMC effectively mitigates the impact of temporary SSR product degradations on positioning accuracy.

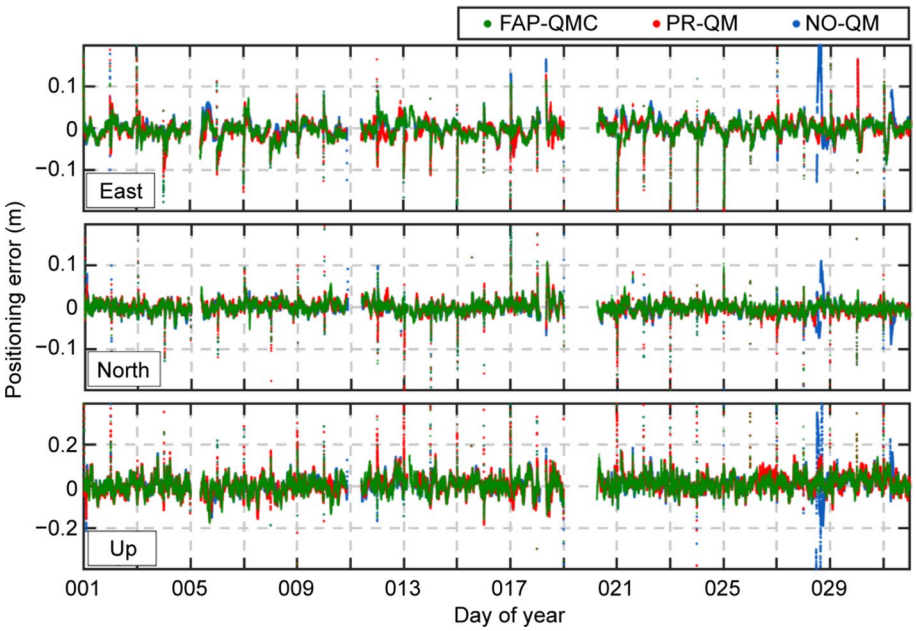

Fig. 7 Positioning errors of ambiguity-float solutions with the FAP-QMC, PR-QM, and NO-QM methods at the station CZDY over one month, 2022

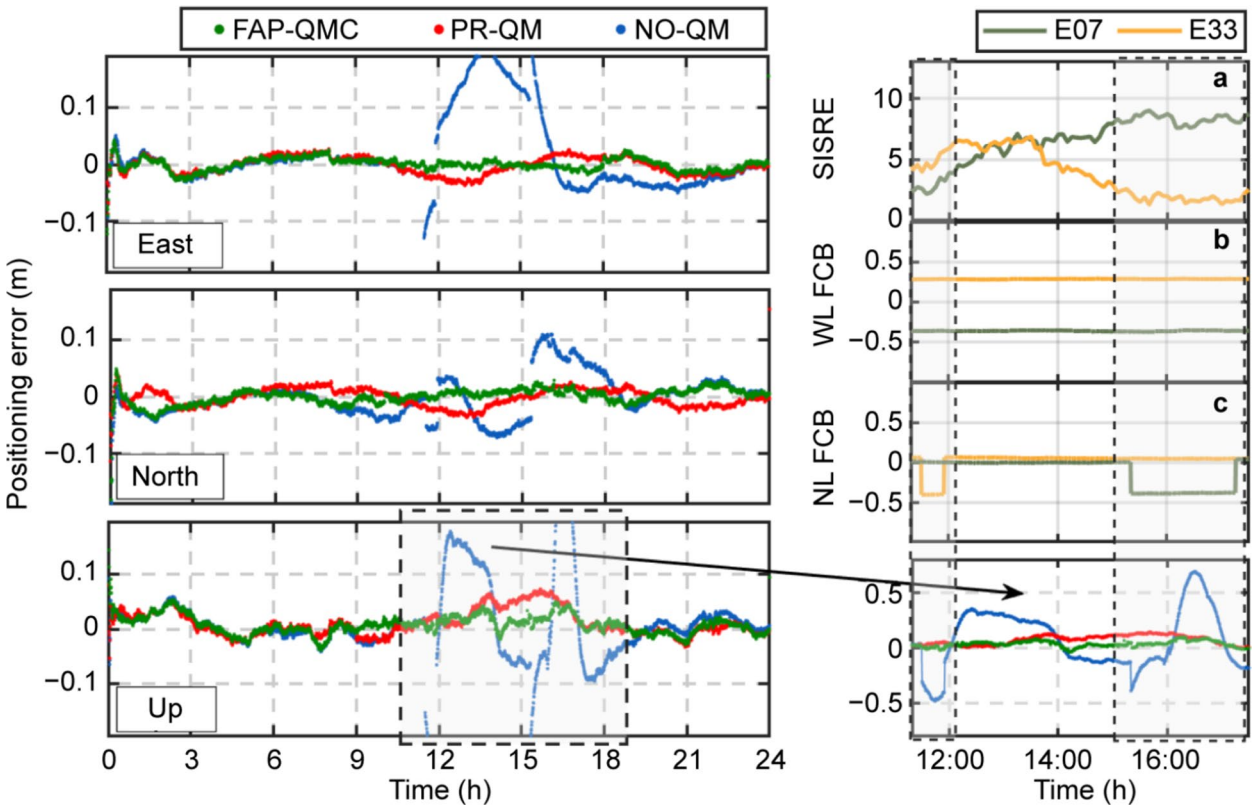

Fig. 8 Positioning errors of ambiguity-float solutions with the FAP-QMC, PR-QM, and NO-QM methods at the station CZDY on DOY 028, 2022 (left panel). The right panel shows SSR product sequences during the period of anomalous positioning: **a** SISRE combined orbit and clock products (cm), **b** WL FCB series in cycles, and **c** NL FCB series in cycles

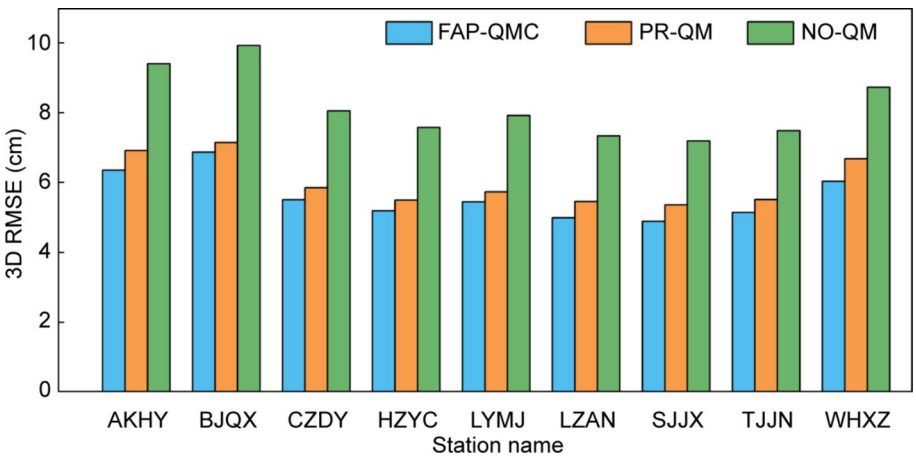

Fig. 9 Average 3D positioning RMSE of ambiguity-float solution with the FAP-QMC, PR-QM, and NO-QM methods. The data were collected from DOY 001 to 031, 2022

Validation in ambiguity-fixed solution

To further validate the effectiveness of the proposed method, PPP-AR was performed using one month of data at nine rover stations (blue circles in Fig. 3) with the FAP-QMC, PR-QM, and NO-QM methods. After the WL and NL float ambiguities were obtained, SD ambiguities were formed to eliminate receiver FCBs. The partial ambiguity resolution strategy was then applied

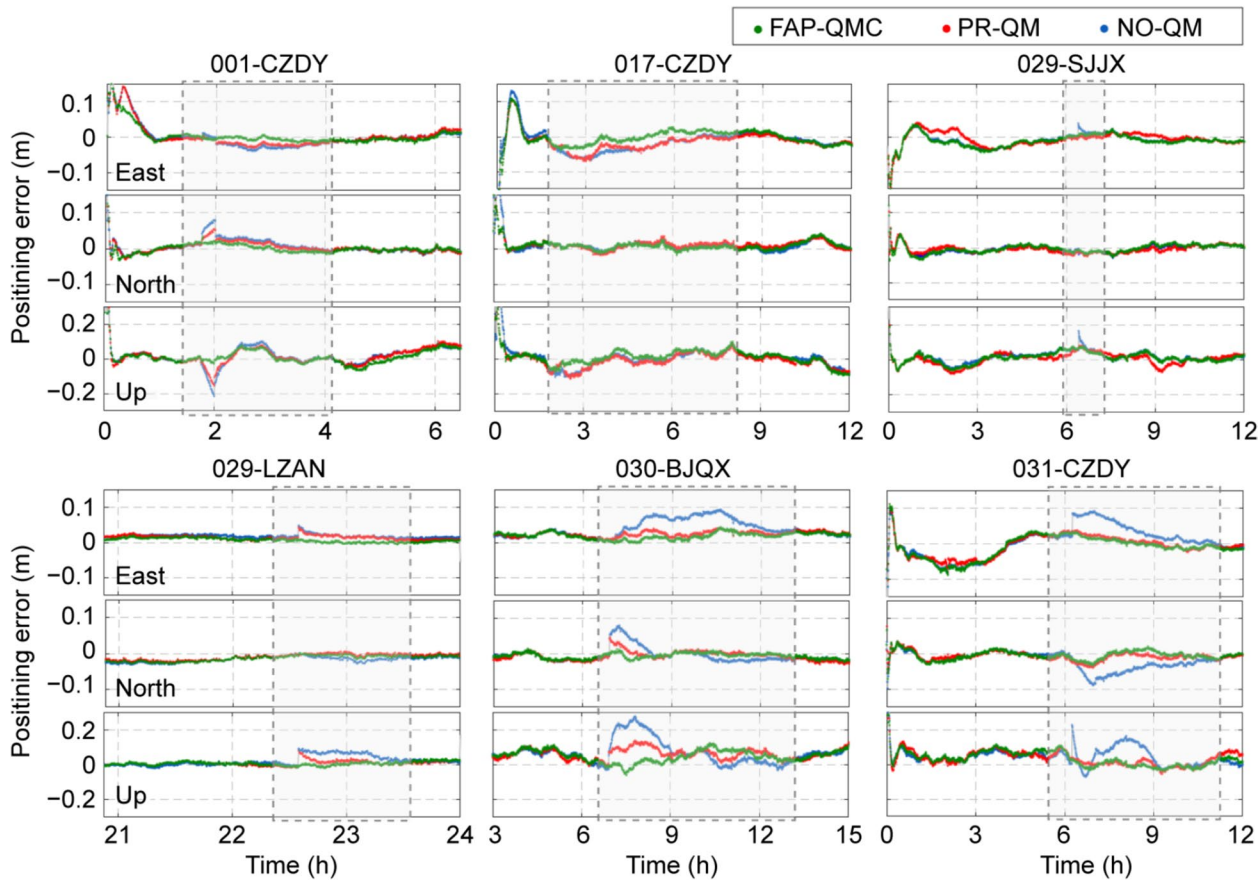

Fig. 10 Positioning error series of ambiguity-float solutions during positioning performance degradation. Results are shown on different days and stations using the FAP-QMC, PR-QM, and NO-QM methods. Within each subplot, the top, middle, and bottom panels correspond to the east, north, and up directions, respectively

to fix the SD WL and NL integer ambiguity using the LAMBDA method, with a success rate of 99.9% and a ratio test threshold of 3.0 (Teunissen, 1995; Verhagen & Teunissen, 2013). Once the WL ambiguities were fixed, the NL ambiguities were subsequently resolved. The performance was evaluated with the indicators of ambiguity fixing rate, incorrect fixing rate, positioning accuracy, and time-to-first-fix.

Figure 11 shows the positioning series at station CZDY on DOY 028, 2022. Significant positioning anomalies, including incorrect ambiguity fixes, are observed between 11:30 and 17:40 with the NO-QM method, while both FAP-QMC and PR-QM methods maintain stable. These anomalies are attributed to SSR product faults during that period. As illustrated in Fig. 8, the PR-QM and the proposed FAP-QMC method effectively excluded the faulty SSR products at the ambiguity-float solution stage, thereby preventing propagation of errors into the ambiguity-fixed solutions. Notably, between 02:30 and 04:00, only FAP-QMC achieved ambiguity-fixed solutions, whereas PR-QM and NO-QM failed to fix the ambiguities. This difference in performance is attributed to the corrections applied by FAP-QMC, which enhance the accuracy of the SSR products (as shown in Fig. 6). Figure 12 compares the SD NL ambiguity deviations during this period. The results show that FAP-QMC achieves smooth and near-zero SD NL ambiguity deviations, creating favorable conditions for ambiguity fixing. In contrast, PR-QM and NO-QM exhibit larger ambiguity deviations. These findings confirm the capability of the FAP-QMC method in anomaly detection and product error mitigation.

The overall ambiguity resolution reliability was evaluated for all stations and the entire testing period. Achieving a high ambiguity fixing rate while minimizing incorrect fixing rate is crucial for high-precision applications such as deformation monitoring and precise navigation, as any incorrect fix can severely compromise reliability. Following this, we define any ambiguity-fixed solution with positioning errors exceeding 10 cm in the East (E), North (N), or Up (U) components as an

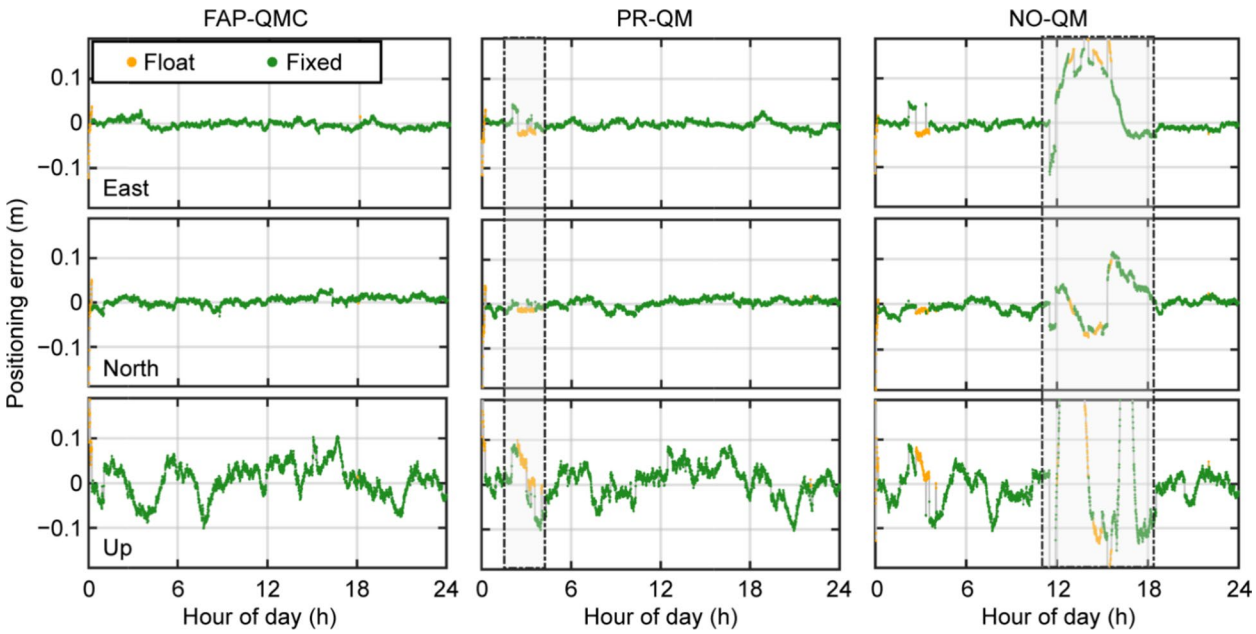

Fig. 11 Positioning errors of ambiguity-fixed solutions with the FAP-QMC (left panel), PR-QM (middle panel), and NO-QM (right panel) methods at station CZDY on DOY 028, 2022. Each panel shows errors in the east (top), north (middle), and up (bottom) directions

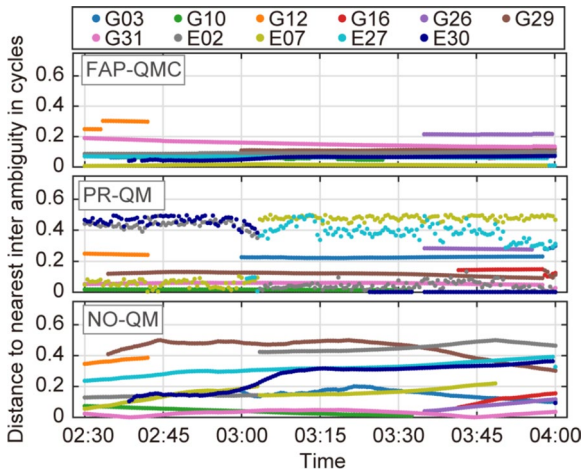

Fig. 12 Distance to integer values of the SD NL ambiguity using the FAP-QMC (top), PR-QM (middle), and NO-QM (bottom) methods at the CZDY station on DOY 028, 2022

incorrect fix, and the incorrect fixing rate is defined as the ratio of epochs with incorrect fixing to the total number of fixed epochs, providing a normalized measure of ambiguity resolution reliability.

Figure 13 summarizes the ambiguity fixing performance for all rover stations over one month. Table 2 gives the corresponding statistical averages for all stations. The NO-QM method achieved an ambiguity fixing rate of 92.50%, with an incorrect fixing rate of 1.48% (1060 epochs). The PR-QM method improved fixing reliability by excluding unreliable SSR products. It achieved a similar fixing rate (92.83%) while reducing the incorrect fixing rate to 0.69% (490 epochs). However, this approach excludes not only truly anomalous products but also all ambiguity-float SSR products, as it cannot effectively assess their quality. Consequently, the average number of fixed satellites decreases by approximately one per epoch compared to NO-QM. In contrast, the proposed FAP-QMC method overcomes these limitations through effective quality assessment and error correction for all SSR products. As shown in Table 2, FAP-QMC achieves the highest ambiguity fixing rate (95.56%), the lowest incorrect fixing rate (0.09%, 69 epochs), and the largest average number of fixed satellites (10.6 per epoch). Compared with the PR-QM method, the proposed FAP-QMC method further increases fixing rate from 92.83 to 95.56% while significantly reduces incorrect fixing rate from 0.69 to 0.09%, demonstrating significant enhancements in both reliability and availability.

Figure 14a displays the one-month 3D positioning RMSE calculated at the epochs when ambiguities were successfully fixed. FAP-QMC achieves the highest accuracy, with an average RMSE of 3.1 cm, while PR-QM and NO-QM achieve 3.8 cm and 5.0 cm, respectively. This overall assessment, however, does not fully reflect the capability of the proposed method in preventing the large positioning errors caused by incorrect ambiguity fixes. Since incorrect ambiguity fixes constitute only

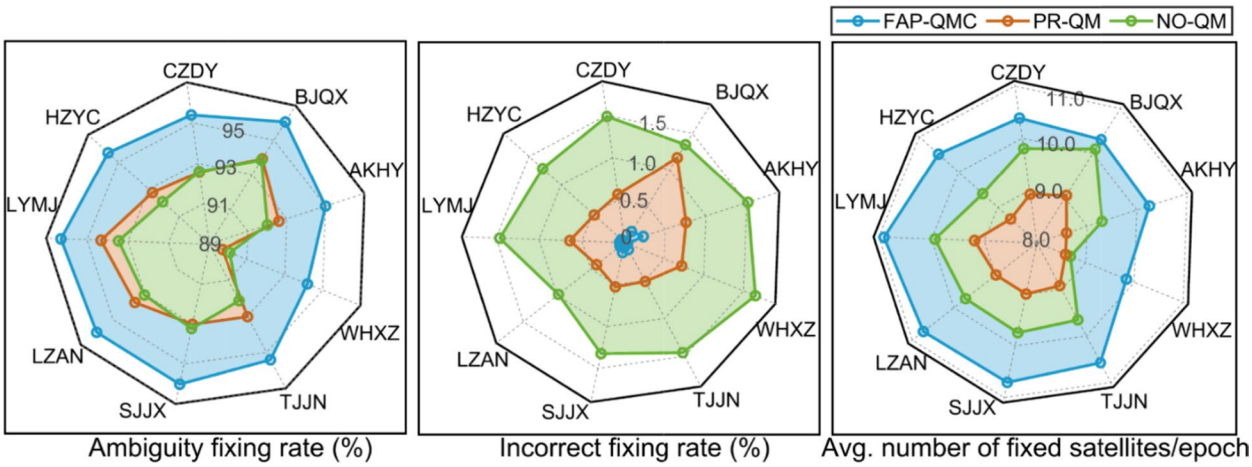

Fig. 13 Ambiguity fixing rate (left), incorrect fixing rate (middle), and average number of fixed satellites per epoch (right) with the FAP-QMC, PR-QM, and NO-QM methods. The data were collected at all rover stations from DOY 001–031, 2022

Table 2 Summary of ambiguity fixing metrics averaged over all rover stations for the one-month period

Method	Ambiguity fixing rate (%)	Average number of satellites fixed per epoch	Incorrect fixing rate (%)	Number of incorrectly fixed epochs
FAP-QMC	95.56	10.6	0.09	69
PR-QM	92.83	8.8	0.69	490
NO-QM	92.50	9.5	1.48	1060

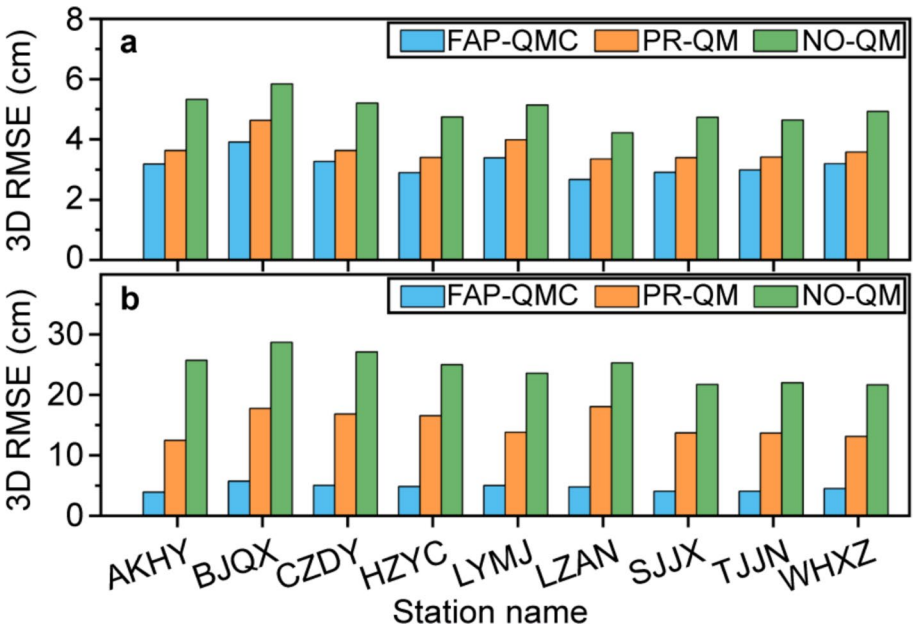

Fig. 14 Average 3D positioning RMSE of ambiguity-fixed solutions with the FAP-QMC, PR-QM, and NO-QM methods: **a** over all epochs; **b** from the epochs with incorrect fixing identified by at least one of the three methods, during DOY 001–031, 2022

a small fraction of total epochs (as shown in Table 2), their impact is diluted in the overall RMSE. Therefore, to specifically evaluate the performance during these critical failure periods, the RMSE was calculated exclusively over the epochs when at least one method resulted in an incorrect fix (Fig. 14b). In this condition, the FAP-QMC method achieves a 3D RMSE of 4.6 cm, compared to 15.1 cm for PR-QM and 24.5 cm for NO-QM. These values correspond to substantial reductions of 10.5 and 19.9 cm, respectively. These results demonstrate that the FAP-QMC method not only delivers superior overall accuracy but also drastically mitigates the impact of incorrect ambiguity fixes, thereby enhancing positioning reliability.

Beyond the positioning accuracy and ambiguity resolution reliability, convergence performance was evaluated using Time-to-First-Fix (TTFF), defined as the time required to obtain the first correct ambiguity-fixed solution after filter initialization. The filter was reset every four hours to obtain multiple TTFF samples.

Figure 15 shows the TTFF cumulative distributions for the three methods. The PR-QM curve lies consistently to the right of both FAP-QMC and NO-QM, with a heavier right tail indicating greater variability. The PR-QM exhibits a median TTFF of 14.0 min, compared to 12.0 min for the FAP-QMC and 13.0 min for the NO-QM. This longer convergence occurs because the PR-QM method excludes likely unreliable SSR products to improve reliability, but this approach also removes ambiguity-float SSR products due to its inability to assess their quality, reducing available satellites and creating a trade-off between reliability and convergence speed. In contrast, the proposed FAP-QMC method evaluates and corrects ambiguity-float SSR products rather than excluding them, thereby preserving more usable satellites (as shown in Fig. 13) and achieving faster convergence without compromising reliability. Table 3 shows 89.97% of FAP-QMC runs converge within 20 min, exceeding the rates of PR-QM and NO-QM by 13.85% and 2.59%, respectively.

Table 3 Proportion of first fixing occurrences within different time intervals

TTFF (min)	FAP-QMC (%)	PR-QM (%)	NO-QM (%)
< 15	70.23	56.25	64.78
< 20	89.97	76.12	87.38
< 25	95.79	85.07	94.02
< 30	97.09	93.28	96.34
< 35	99.00	96.64	98.65

The preceding analyses, conducted under normal observation conditions, demonstrated that the proposed FAP-QMC method significantly improved PPP-AR reliability compared to the traditional PR-QM method. To further assess the applicability of FAP-QMC under satellite-limited conditions, one-month simulation experiments were conducted. The experiments involved randomly removing four satellite observations per epoch with the set of unavailable satellites rotated dynamically every two hours, and simulating complete signal loss for all satellites once every four hours, thereby emulating

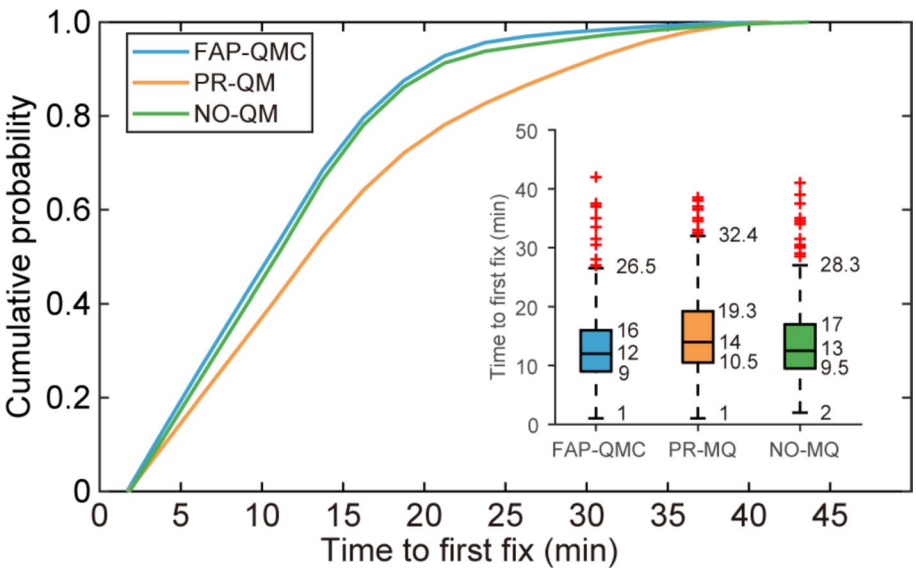

Fig. 15 TTFF distributions with the three methods, showing Cumulative Distribution Functions (CDFs) and boxplots using the data at nine rover stations over one month. The boxplots indicate the median, quartiles, and bounds calculated by (14) for each method

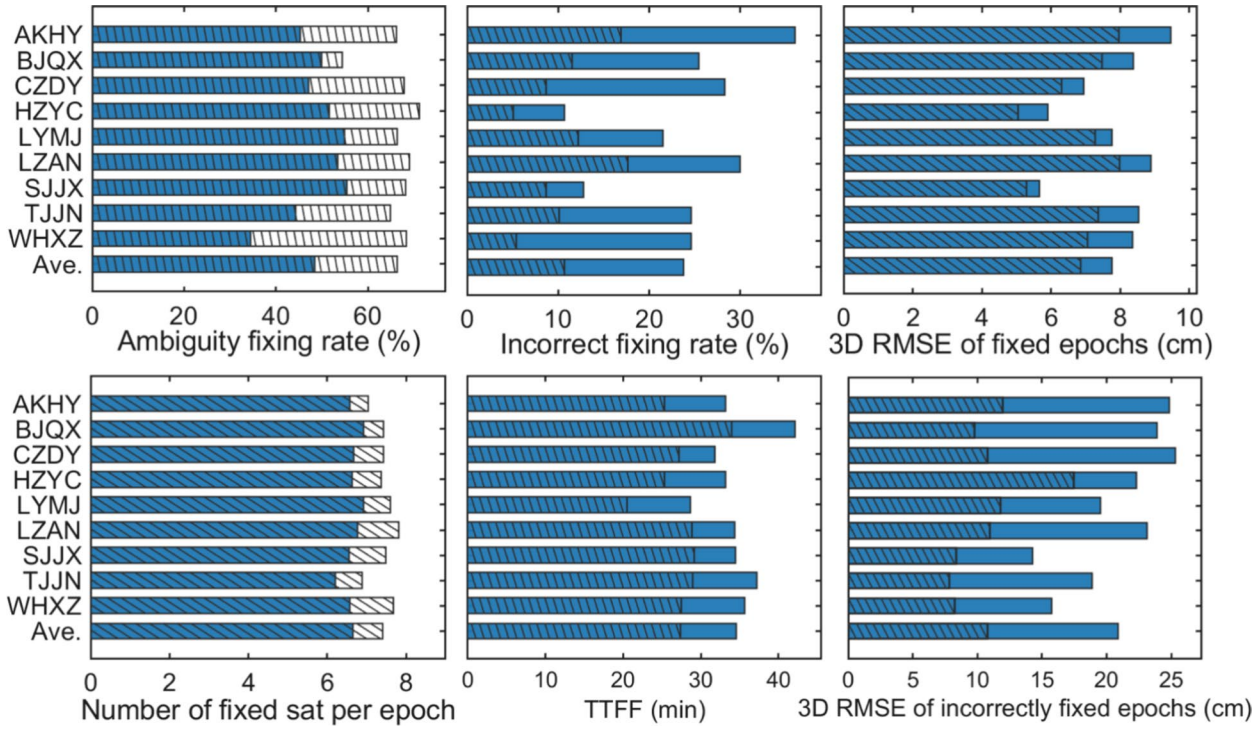

Fig. 16 Positioning performance of FAP-QMC and PR-QM under satellite-limited observation conditions. The shaded and solid bars represent the results of using FAP-QMC and PR-QM methods, respectively

challenging scenarios such as tunnel passages or severe urban obstruction.

Figure 16 shows the positioning performance of FAP-QMC and PR-QM under these conditions. The PR-QM method ensures SSR product quality by excluding potentially unreliable products, which reduces the number of satellites available for ambiguity resolution. The FAP-QMC method, through its monitoring and correction strategy, preserves and corrects more ambiguity-float satellite observations while maintaining SSR product reliability, thereby enabling the use of approximately one additional satellite per epoch for ambiguity fixing. Under these conditions, FAP-QMC achieves an ambiguity fixing rate of 66.26% (vs. 48.43% for PR-QM), an incorrect fixing rate of 10.34% (vs. 22.66% for PR-QM), and a median TTFF of 27.43 min (vs. 34.53 min for PR-QM). Additionally, FAP-QMC reduces the 3D RMSE during incorrectly fixed epochs, demonstrating improved positioning accuracy across all scenarios. These results indicate that FAP-QMC exhibits better adaptability in maintaining solution availability and reliability in resource-constrained complex environments. It is worth noting that under such severely constrained conditions, the overall performance of both methods declines, and future research should further investigate how to enhance PPP-AR robustness under more extreme conditions.

Conclusions

This study establishes that in float PPP, combined SSR product errors are distributed between float ambiguity deviations and phase residuals. Building on this principle, a new monitoring and correction method for combined SSR product errors has been developed. The method overcomes the limitation of the traditional monitoring approaches based on ambiguity-fixed phase residuals, which cannot reliably assess the actual error levels of ambiguity-float SSR products. By jointly considering float ambiguity deviations and ambiguity-float phase residuals as quality indicators, the proposed method provides a comprehensive characterization of combined SSR product errors and is applicable to both ambiguity-float and ambiguity-fixed SSR products. Moreover, by integrating spatial error modeling of float ambiguity deviations, the method extends beyond simple monitoring, as it can provide both product error correction and anomaly alerts to PPP-AR users. These capabilities collectively advance the state of the art in SSR quality management.

The validation of the method has been conducted using one month of real-time SSR products in a wide-area network, incorporating GPS (L1 + L2) and Galileo (E1 + E5a), and demonstrates significant performance improvements. Compared to the traditional method based on ambiguity-fixed phase residuals, the proposed

method increases the ambiguity fixing rate from 92.83 to 95.56% while reducing the incorrect fixing rate from 0.69 to 0.09%. These improvements significantly reduce positioning errors during incorrect fixed epochs, with the 3D RMSE decreasing from 15.1 to 4.6 cm. Importantly, these improvements are achieved without the trade-off faced by the traditional methods based on ambiguity-fixed phase residuals, which gain reliability by excluding anomalous SSR products but also exclude ambiguity-float SSR products, resulting in a reduction of 1 to 2 usable satellites per epoch and, consequently, an increase in the median TTFF from 13 to 14 min. In contrast, the proposed method recovers some of these excluded but usable SSR products and further improves the quality of all SSR products by deriving error corrections for them. As a result, the method provides both faster TTFF and higher reliability than traditional methods.

This performance difference becomes more noticeable in challenging environments. While the performance of both methods declines under these extreme conditions, the proposed method still maintains a clear advantage. Under a simulated condition of frequent signal interruptions and loss of satellite lock, the median TTFF of the proposed method is reduced from 34.53 to 27.43 min, the ambiguity fixing rate increases from 48.43 to 66.26%, and the incorrect fixing rate decreases from 22.66% to 10.34%. In summary, the proposed method enhances the reliability and availability of SSR products, providing a robust and practical solution for real-time high-precision PPP-AR applications in both research and operational contexts.

Abbreviations

PPP-AR	Precise point positioning with ambiguity resolution
SSR	State space representation
SISRE	Signal in space range errors
IF	Ionosphere-free
OSB	Observable-specific signal bias
FCB	Fractional cycle biases
SD	Satellite-differenced
IQR	Interquartile range
DBSCAN	Density-based spatial clustering of applications with noise
WSTD	Weighted standard deviation
RMSE	Root mean square error
TTFF	Time-to-first-fix
FAP-QMC	Float-ambiguity deviation and phase residual-based quality monitoring and correction
PR-QM	Phase residual-based quality monitoring
NO-QM	No quality monitoring

Acknowledgements

We appreciate the Geespace Company collecting the GNSS data, which made the experiment possible.

Author contributions

Yunqing Tian and Bao Shu conceived the study and designed the experiments. Yuhang Zheng and Yunqing Tian performed the experiments and drafted the original manuscript. Bao Shu, Guillermo González-Casado, Yang Gao, Li Wang and Adria Rovira-Garcia contributed to conceptualization, formal analysis, and manuscript revision. Guanwen Huang, Qin Zhang reviewed and revised the manuscript.

Funding

This work is funded by the National Natural Science Foundation of China (42127802; 42004024), the Natural Science Basic Research Program of Shanxi Province (2025JC-YBMS-251), the innovation team of Shaanxi Provincial Tri-Qin Scholars with Geoscience Big Data and Geohazard Prevention (2022), and the Fundamental Research Funds for the Central Universities, CHD (300102263202; 300102263714). Guillermo González-Casado acknowledges support from project PID2022-138485OB-I00 funded by MCIN/AEI/https://doi.org/10.13039/501100011033/FEDER, UE.

Data availability

The real-time orbit, clock, and OSB products were downloaded from the Centre National d'Etudes Spatiales (http://www.ppp-wizard.net/products/REAL_TIME/), and the GNSS observations are available from the corresponding author on reasonable request.

Declarations

Competing interests

The authors declare that they have no conflict of interest.

Author details

[1]College of Geological Engineering and Geomatics, Chang'an University, Xi'an 710054, China. [2]Research Group of Astronomy and Geomatics (gAGE), Universitat Politecnica de Catalunya (UPC), Barcelona, Spain. [3]Department of Geomatics Engineering, University of Calgary, Calgary, Canada.

Received: 5 November 2025 Revised: 28 March 2026 Accepted: 30 March 2026
Published online: 13 April 2026

References

Baarda, W. (1968). A testing procedure for use in geodetic networks. *Netherlands geodetic commission, 2*(5). https://doi.org/10.54419/t8w4sg.

Banville, S., Geng, J., Loyer, S., Schaer, S., Springer, T., & Strasser, S. (2020). On the interoperability of IGS products for precise point positioning with ambiguity resolution. *Journal of Geodesy, 94*(1), 1–15. https://doi.org/10.1007/s00190-019-01335-w

Du, S., Shu, B., Xie, W., Huang, G., Ge, Y., & Li, P. (2022). Evaluation of real-time precise point positioning with ambiguity resolution based on Multi-GNSS OSB products from CNES. *Remote Sensing, 14*(19), Article 4970. https://doi.org/10.3390/rs14194970

Du, Y., Wang, J., Rizos, C., & El-Mowafy, A. (2021). Vulnerabilities and integrity of precise point positioning for intelligent transport systems: Overview and analysis. *Satellite Navigation, 2*(1), Article 3. https://doi.org/10.1186/s43020-020-00034-8

Duan, B., Hugentobler, U., Chen, J., Selmke, I., & Wang, J. (2019). Prediction versus real-time orbit determination for GNSS satellites. *GPS Solutions, 23*(2), Article 39. https://doi.org/10.1007/s10291-019-0834-2

Duan, B., Hugentobler, U., & Montenbruck, O. (2024). A method to assess the quality of GNSS satellite phase bias products. *GPS Solutions, 28*(2), Article 89. https://doi.org/10.1007/s10291-024-01634-6

Ester, M., Kriegel, H.-P., Sander, J., & Xu, X. (1996). A density-based algorithm for discovering clusters in large spatial databases with noise. In *kdd* (pp. 226–231).

Fujita, S., Sato, Y., Miya, M., Ota, K., Hirokawa, R., & Takiguchi, J.-i. (2016). Design of Integrity Function on Centimeter Level Augmentation Service (CLAS) in Japanese Quasi-Zenith Satellite System. In *Proceedings of the 29th International Technical Meeting of the Satellite Division of the Institute of Navigation (ION GNSS+ 2016)* (pp. 3258–3263). https://doi.org/10.33012/2016.14571.

Gao, R., Ye, F., Liu, Y., Zha, J., Odolinski, R., Satirapod, C., & Zhang, B. (2024). Optimizing ZWD estimation strategies for enhanced PPP-RTK performance. *GPS Solutions, 28*(2), Article 86. https://doi.org/10.1007/s10291-024-01629-3

Ge, M., Gendt, G., Rothacher, M., Shi, C., & Liu, J. (2008). Resolution of GPS carrier-phase ambiguities in precise point positioning (PPP) with daily observations. *Journal of Geodesy, 82*(7), 389–399. https://doi.org/10.1007/s00190-007-0187-4

Hatch, R. (1983). The synergism of GPS code and carrier measurements. In *International Geodetic Symposium on Satellite Doppler Positioning* (pp. 1213–1231).

Huang, J., Li, X., Li, X., Wu, J., Zhang, K., Yuan, Y., & Zhang, W. (2024). Real-time outlier detection of satellite orbit and clock products using reverse error estimation. *GPS Solutions, 29*(1), Article 2. https://doi.org/10.1007/s10291-024-01753-0

Ji, R., Jiang, X., Chen, X., Zhu, H., Ge, M., & Neitzel, F. (2022). Quality monitoring of real-time GNSS precise positioning service system. *Geo-Spatial Information Science*, *26*(1), 1–15. https://doi.org/10.1080/10095020.2022.2070554

Khan, K., Rehman, S. U., Aziz, K., Fong, S., & Sarasvady, S. (2014). DBSCAN: Past, present and future. In *The fifth international conference on the applications of digital information and web technologies (ICADIWT 2014)* (pp. 232–238). https://doi.org/10.1109/ICADIWT.2014.6814687.

Laurichesse, D. (2012). Phase biases estimation for undifferenced ambiguity resolution. In *PPP-RTK & Open Standards Symposium* (pp. 12–13).

Laurichesse, D., Mercier, F., Berthias, J. P., Broca, P., & Cerri, L. (2009). Integer ambiguity resolution on undifferenced GPS phase measurements and its application to PPP and satellite precise orbit determination. *Navigation, 56*(2), 135–149. https://doi.org/10.1002/j.2161-4296.2009.tb01750.x

Li, B., Ge, H., Bu, Y., Zheng, Y., & Yuan, L. (2022). Comprehensive assessment of real-time precise products from IGS analysis centers. *Satellite Navigation, 3*(1), Article 12. https://doi.org/10.1186/s43020-022-00074-2

Li, X., Huang, J., Li, X., Lyu, H., Wang, B., Xiong, Y., & Xie, W. (2021). Multi-constellation GNSS PPP instantaneous ambiguity resolution with precise atmospheric corrections augmentation. *GPS Solutions, 25*(3), Article 107. https://doi.org/10.1007/s10291-021-01123-0

Li, X., Liang, D., Li, X., Huang, J., Wu, J., & Gou, H. (2024). Quality monitoring of real-time PPP service using isolation forest-based residual anomaly detection. *GPS Solutions, 28*(3), Article 118. https://doi.org/10.1007/s10291-024-01657-z

Liu, T., Jiang, W., Laurichesse, D., Chen, H., Liu, X., & Wang, J. (2020). Assessing GPS/Galileo real-time precise point positioning with ambiguity resolution based on phase biases from CNES. *Advances in Space Research, 66*(4), 810–825. https://doi.org/10.1016/j.asr.2020.04.054

Lou, Y., Zhang, W., Wang, C., Yao, X., Shi, C., & Liu, J. (2014). The impact of orbital errors on the estimation of satellite clock errors and PPP. *Advances in Space Research, 54*(8), 1571–1580. https://doi.org/10.1016/j.asr.2014.06.012

Melbourne, W. G. (1985). The case for ranging in GPS-based geodetic systems. In *Proceedings of the first international symposium on precise positioning with the Global Positioning System* (pp. 373–386).

Montenbruck, O., Steigenberger, P., & Hauschild, A. (2018). Multi-GNSS signal-in-space range error assessment - Methodology and results. *Advances in Space Research, 61*(12), 3020–3038. https://doi.org/10.1016/j.asr.2018.03.041

Rousseeuw, P. J., & Hubert, M. (2018). Anomaly detection by robust statistics. *Wiley Interdisciplinary Reviews: Data Mining and Knowledge Discovery, 8*(2), Article e1236. https://doi.org/10.1002/widm.1236

Sanz, J., Juan, J., & Hernández-Pajares, M. (2013). *GNSS data processing volume i: Fundamentals and algorithms, vol. i*. ESA Communications.

Shu, B., Liu, H., Wang, L., Huang, G., Zhang, Q., & Yang, Z. (2021). Performance improvement of real-time PPP ambiguity resolution using a regional integer clock. *Advances in Space Research, 67*(5), 1623–1637. https://doi.org/10.1016/j.asr.2020.12.012

Shu, B., Tian, Y., Qu, X., Li, P., Wang, L., Huang, G., Du, Y., & Zhang, Q. (2024). Estimation of BDS-2/3 phase observable-specific signal bias aided by double-differenced model: An exploration of fast BDS-2/3 real-time PPP. *GPS Solutions, 28*(2), Article 88. https://doi.org/10.1007/s10291-024-01632-8

Teunissen, P. J. G. (1995). The least-squares ambiguity decorrelation adjustment: A method for fast GPS integer ambiguity estimation. *Journal of Geodesy, 70*(1), 65–82. https://doi.org/10.1007/BF00863419

Teunissen, P. J. G. (2018). Distributional theory for the DIA method. *Journal of Geodesy, 92*(1), 59–80. https://doi.org/10.1007/s00190-017-1045-7

Teunissen, P. J., Odijk, D., & Zhang, B. (2010). PPP-RTK: Results of CORS network-based PPP with integer ambiguity resolution. *Journal of Aeronautics, Astronautics and Aviation. Series A, 42*(4), 223–230.

Tian, Y., Shu, B., Gao, Y., Huang, G., Li, P., Zhang, Q., & Wang, L. (2025). Analysis and comparison of FCB and IRC models considering effect of real-time orbit and clock product errors. *GPS Solutions, 29*(3), Article 133. https://doi.org/10.1007/s10291-025-01879-9

Verhagen, S., & Teunissen, P. J. G. (2013). The ratio test for future GNSS ambiguity resolution. *GPS Solutions, 17*(4), 535–548. https://doi.org/10.1007/s10291-012-0299-z

Vinutha, H., Poornima, B., & Sagar, B. (2018). Detection of outliers using interquartile range technique from intrusion dataset. In *Information and decision sciences: Proceedings of the 6th international conference on ficta* (pp. 511–518). https://doi.org/10.1007/978-981-10-7563-6_53.

Wang, Y., Li, R., & Zhao, R. (2015). Research of signal-in-space integrity monitoring based on inter-satellite links. *Chinese Journal of Electronics, 24*(2), 439–444. https://doi.org/10.1049/cje.2015.04.036

Wang, Y., & Shen, J. (2020). Real-time integrity monitoring for a wide area precise positioning system. *Satellite Navigation, 1*(1), Article 24. https://doi.org/10.1186/s43020-020-00018-8

Weber, G., Mervart, L., Lukeš, Z., Rocken, C., & Douša, J. (2007). Real-time Clock and Orbit Corrections for Improved Point Positioning via NTRIP. In *Proceedings of the 20th international technical meeting of the satellite division of the institute of navigation (ION GNSS 2007)* (pp. 1992–1998).

Weinbach, U., Brandl, M., Chen, X., Landau, H., Pastor, F., Reussner, N., & Rodriguez-Solano, C. (2018). Integrity of the Trimble® centerpoint RTX correction service. In *Proceedings of the 31st International Technical Meeting of The Satellite Division of the Institute of Navigation (ION GNSS+ 2018)* (pp. 1902–1909). https://doi.org/10.33012/2018.15971.

Wübbena, G. (1985). Software developments for geodetic positioning with GPS using TI-4100 code and carrier measurements. In *Proceedings of the first international symposium on precise positioning with the global positioning system* (pp. 403–412).

Xiao, G., Xiao, Z., Zhou, P., Liu, C., Wei, H., & Li, P. (2025). Performance evaluation of Galileo high accuracy service for PPP ambiguity resolution. *GPS Solutions, 29*(3), Article 96. https://doi.org/10.1007/s10291-025-01852-6

Xie, M., Wang, N., El-mowafy, A., Li, Z., Liu, A., & Wei, D. (2025). Characterizing PPP ambiguity resolution residuals for precise orbit and clock corrections integrity monitoring. *GPS Solutions, 29*(2), Article 69. https://doi.org/10.1007/s10291-025-01827-7

Xue, Y., Zheng, F., Zhou, G., Chao, W., Zhang, D., & Shi, C. (2024). A new quality monitoring method for real-time precise orbit and clock products. *GPS Solutions, 28*(3), Article 125. https://doi.org/10.1007/s10291-024-01673-z

Zhang, Y., Kubo, N., Chen, J., Wang, J., & Wang, H. (2019). Initial positioning assessment of BDS new satellites and new signals. *Remote Sensing, 11*(11), 1320. https://doi.org/10.3390/rs11111320

Zheng, K., Zhang, X., Sang, J., Zhao, Y., Wen, G., & Guo, F. (2021). Common-mode error and multipath mitigation for subdaily crustal deformation monitoring with high-rate GPS observations. *GPS Solutions, 25*(2), Article 67. https://doi.org/10.1007/s10291-021-01095-1

Zhou, G., Zheng, F., & Shi, C. (2025). Development and validation of an integrity monitoring framework of real-time PPP correction data. *Chinese Journal of Aeronautics*. https://doi.org/10.1016/j.cja.2025.103434

Zhou, P., Xiao, G., & Du, L. (2023). Initial performance assessment of Galileo High Accuracy Service with software-defined receiver. *GPS Solutions, 28*(1), Article 2. https://doi.org/10.1007/s10291-023-01540-3

Publisher's Note